NOTE *Virology*

Inhibitory Effect of Newly Developed CXC-Chemokine Receptor 4 Antagonists on the Infection with Feline Immunodeficiency Virus

Fuminori MIZUKOSHI[1], Kenji BABA[1], Yuko GOTO-KOSHINO[1], Asuka SETOGUCHI-MUKAI[1], Yasuhito FUJINO[1], Koichi OHNO[1], Hirokazu TAMAMURA[2], Shinya OISHI[3], Nobutaka FUJII[3] and Hajime TSUJIMOTO[1]*

[1]*Department of Veterinary Internal Medicine, Graduate School of Agricultural and Life Sciences, The University of Tokyo, 1–1–1 Yayoi, Bunkyo-ku, Tokyo 113–8657,* [2]*Institute of Biomaterials and Bioengineering, Tokyo Medical and Dental University, Chiyoda-ku, Tokyo 101–0062 and* [3]*Graduate School of Pharmaceutical Sciences, Kyoto University, Sakyo-ku, Kyoto 606–8501, Japan*

(Received 16 November 2007/Accepted 29 September 2008)

ABSTRACT. CXC-chemokine receptor 4 (CXCR4) functions as a receptor for feline immunodeficiency virus (FIV). Although we previously found that a CXCR4 antagonist, T140, inhibited the FIV replication *in vitro*, it was not effective in cats infected with FIV because of its low stability in feline serum. To resolve this problem, several T140 derivatives have been developed. Here, we examined the efficacy of T140 analogs, TF14016 and TF14013, on the inhibition of FIV infection. These compounds were shown to significantly inhibit the syncytia formation in CXCR4-expressing cells after co-cultivation with FIV-infected cells and the replication of FIV in a feline lymphoid cultured cell line. These results indicated that TF14016 and TF14013 could be useful as antiviral drugs for cats infected with FIV.

KEY WORDS: CXCR4 antagonist, feline, FIV.

J. Vet. Med. Sci. 71(1): 121–124, 2009

CXC-chemokine receptor 4 (CXCR4) is one of the co-receptors for human immunodeficiency virus (HIV) and feline immunodeficiency virus (FIV) and necessary for the cell entry of both viruses [2, 3, 16, 23]. Therefore, blockade of CXCR4 has been expected to be a novel therapeutic strategy in HIV and FIV infections. Previous studies using a natural ligand for CXCR4, stromal cell derived factor-1 (SDF-1), revealed its inhibitory effect against HIV and FIV infections by blocking CXCR4 [4, 5, 8, 10, 16], but indicated its problematic side effect such as marked inflammation after injection *in vivo* [13]. Several CXCR4 antagonists, AMD3100, T22 and T140, were also shown to inhibit HIV infection [6, 7, 17] in cultured cells, but there is no report showing their clinical use because of their instability and strong side effect *in vivo*.

T22 is a derivative of a peptide derived from horseshoe crab blood cells [12]. This peptide consisting of 18-amino acid residues binds specifically to CXCR4 on human cells and inhibits the entry of HIV, however, it does not activate the target cells. Its derivative, T140, is unstable due to the cleavage of C-terminal Arg^{14} in serum and liver homogenate. However, the C-terminally amidated analogs of T140, TF14016 and TF14013, were shown to be bio-stable by virtue of stabilization of the Arg^{14} and possess high antiviral activity, low cytotoxicity, and *in vivo* stability [19]. In this study, we examined the inhibitory effect of TF14016 and TF14013 on the infection with FIV in cultured cells. These compounds were prepared as described previously [19] (Table 1). They were dissolved in water at 1 mM and kept in a freezer at –20°C until use for the assays.

First, we investigated whether TF14016 and TF14013 interact with feline CXCR4. The 3201 cells, which showed strong expression of cell surface CXCR4, were pretreated with 4 μM of these compounds on ice for 30 min. Then, these cells were reacted with an anti-CXCR4 monoclonal antibody (clone 44717) (R & D systems, Minneapolis, MN) in flow cytometric analysis (FCM) buffer (2% fetal calf serum in PBS) on ice for 30 min. The cells were washed twice with FCM buffer and then incubated with fluorescein isothiocyanate (FITC)-conjugated goat anti-mouse IgG antibody for 30 min on ice. The cells were washed twice with FCM buffer and analyzed with a flow cytometer (FACSCalibur) (Becton Dickinson Immunocytometry systems, San Jose, CA). The fluorescence intensity of 3201 cells detected by clone 44717 was remarkably diminished when the cells were preincubated with both of the compounds (Fig. 1). Clone 44717 was shown to bind to the extracellular loop 2 (E-L2) region of human and feline CXCR4 in the N-terminal domain [1]. The previous report showed that T140 compounds physically bind to E-L2 region of human CXCR4 [22]. Moreover, the E-L2 region was shown to be the most important site in feline CXCR4 for the interaction with FIV envelope protein [23]. Consequently, it is conceivable that the masking of E-L2 region with the T140 analogs results in

Table 1. Amino acid sequence of T140 analogs

TF14016 4F-benzoly-Arg-Arg-Nal-Cys-Try-Cit-Lys-DLys-Pro-Tyr-Arg-Cit-Cys-Arg-NH_2
TF14013 4F-benzoly-Arg-Arg-Nal-Cys-Try-Cit-Lys-DGlu-Pro-Tyr-Arg-Cit-Cys-Arg-NH_2

* CORRESPONDENCE TO: TSUJIMOTO, H., Department of Veterinary Internal Medicine, Graduate School of Agricultural and Life Sciences, The University of Tokyo, 1–1–1 Yayoi, Bunkyo-ku, Tokyo 113–8657, Japan.
e-mail: atsuji@mail.ecc.u-tokyo.ac.jp

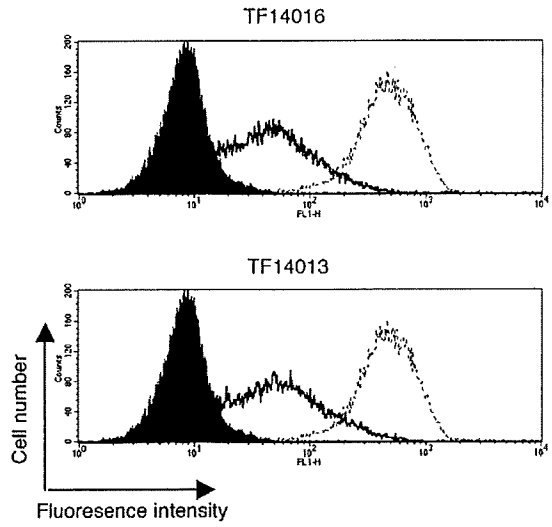

Fig. 1. Fow cytometric analysis to show the inhibitory effect of TF14016 and TF14013 on the binding of anti-CXCR4 monoclonal antibody in 3201 cells. The 3201 cells were treated with the anti-CXCR4 antibody in the presence (thick solid line) or absence (light solid line) of each compound (4 μM). As a control, the 3201 cells were treated with an isotype control antibody (filled histogram). Then, these cells were treated with FITC-conjugated anti-mouse IgG as a secondary antibody for the flow cytometric analysis.

the interference of the interaction between CXCR4 and FIV envelope protein.

HeLa cells were seeded in Dulbecco's Modified Eagle's Medium (DMEM) and cultured overnight to form monolayers. On the following day, TF14016 or TF14013 (4 μM each) was added, and the cells were cultured at 37°C for 1 hr. Then, CRFK/FIV cells [15] were added into each of the wells. After 24 hr, the cells were fixed with methanol and stained with Wright and Giemsa solutions. After co-cultivation with CRFK/FIV cells, a number of syncytia were observed as reported by Willet *et al.* [23]. When the HeLa cells were pretreated with either TF14016 or TF14013, the syncytia formation in HeLa cells after co-cultivation with CRFK/FIV cells was remarkably inhibited (Fig. 2). Syncytia formation inhibition rates by the treatment with TF14016 and TF14013 (4 μM) were 98.1% and 96.2%, respectively, which were calculated as [(number of syncytia in the presence of the compound–number of spontaneously formed syncytia)/(number of syncytia in the absence of the compounds–number of spontaneously formed syncytia) × 100].

Inhibitory effect of the CXCR4 antagonists on the replication of FIV was examined in Kumi-1 cells which were highly permissive to FIV infection [9]. Prior to the experiment, the CXCR4 antagonists were shown to induce no cytotoxic effect on Kumi-1 cells at their concentrations up to 4 μM. Kumi-1 cells (2×10^6 cells/m*l*) were first treated with each of the CXCR4 antagonist compounds, TF14016 and TF14013 (4 μM), at 37°C for 1 hr, and then inoculated with a subtype A FIV strain, Sendai-1 [11] (final concentration of reverse transcriptase (RT) activity, 50,000 cpm/m*l*).

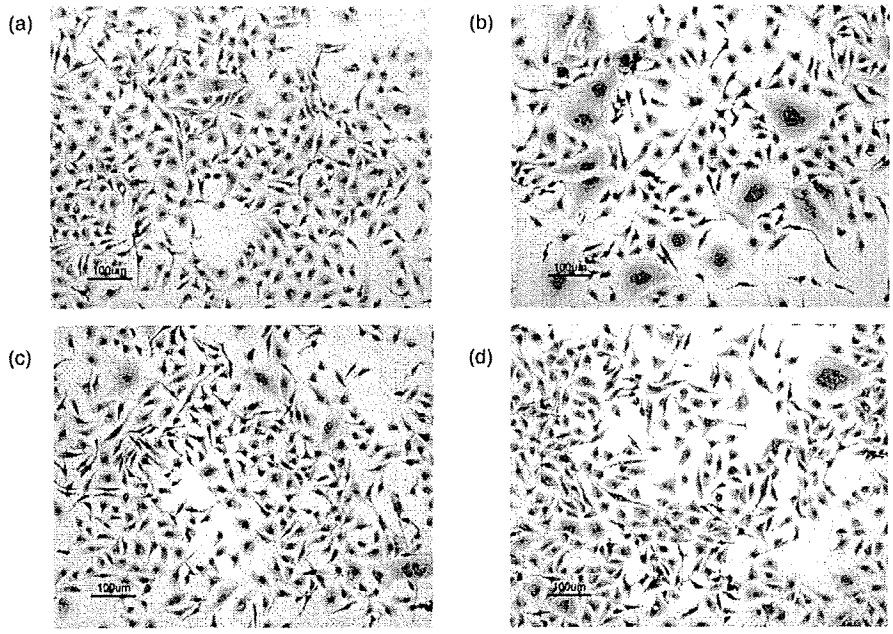

Fig. 2. Inhibition of FIV-mediated syncytia in HeLa cells by the treatment with CXCR4 antagonists. (a) HeLa cells. (b) HeLa cells after cocultivation with CRFK/FIV cells. HeLa cells pretreated with a CXCR4 antagonist, TF14016 (c) or TF14013 (d) (4 μM), succeedingly co-cultured with CRFK/FIV cells.

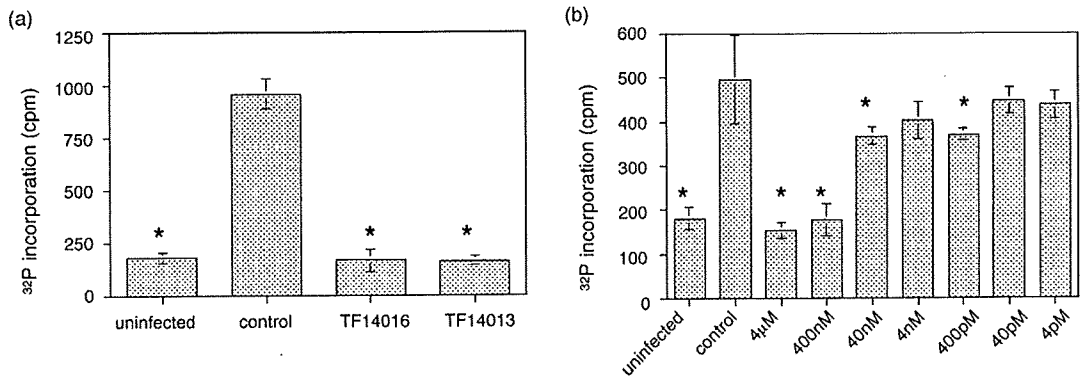

Fig. 3. Inhibitory effect of TF14016 and TF14013 on the replication of FIV in Kumi-1 cells. (a) Untreated Kumi-1 cells (control) and those treated with 4 μM of TF14016 or TF14013 were inoculated with the FIV Sendai-1 strain. RT activity in the culture supernatants was measured 6 days after inoculation with FIV. RT activity in the culture supernatant of uninfected Kumi-1 cells is also shown (uninfected). (b) Dose-dependency of the antiviral effect of TF14016 on the replication of FIV in Kumi-1 cells. The columns and bars show mean and standard deviations, respectively. Asterisks indicate significant difference from the RT value in the untreated Kumi-1 cells inoculated with FIV.

After adsorption at 37°C for 3 hr, the cells were washed twice with PBS and resuspended to a final cell density of 5 x 10^5 cells/m*l*. The cells were cultured in RPMI-1640 medium supplemented with 100 U of human recombinant interleukin-2 (Pharma Biotechnologie, Hannover, Germany) per m*l*. They were passaged 3 days later to dilute the cell density to 5 x 10^5 cells/m*l* and were added with each of the fresh compounds. The cell-free supernatants were harvested 6 days after inoculation with FIV to measure RT activity as described previously [8]. When the Kumi-1 cells were pretreated with TF14016 (4 μM) or TF14013 (4 μM), the replication of FIV in Kumi-1 cells was significantly inhibited as shown by the decrease of RT activity in their culture supernatants (Fig. 3a). The TF14016 was shown to decrease the RT-activity in the supernatants of the FIV-infected Kumi-1 cells in a dose-dependent manner (Fig. 3b).

The C-terminally amidated analogs of T140 as used in this study were shown to have a potential efficacy against HIV infection [19] as well as rheumatoid arthritis and tumor metastasis mouse models [18, 20]. Additionally, previous studies demonstrated that these compounds were considerably stable in feline serum [21] and effectively inhibited feline SDF-1-induced migration of a feline mammary tumor cell line [14]. In this study, these compounds were shown to significantly inhibit FIV replication at the cell entry level. Thus, it is reasonable to suppose that the administration of these new T140 analogs may exert their antiviral effect in cats infected with FIV. However, because the inhibitory effect of T140 analogs against FIV infection was observed at concentrations more than 400 nM, clinically achievable blood levels remain as a matter to be investigated. Further study is needed to examine the *in vivo* bioavailability, efficacy, and toxicity of the new T140 analogs before their clinical application in cats infected with FIV.

ACKNOWLEDGEMENT. This study was supported by grants from the Japan Health Science Foundation and the Ministries of Education, Science, Sports and Culture, and Health and Welfare of Japan.

REFERENCES

1. Baribaud, F., Edwards, T. G., Sharron, M., Brelot, A., Heveker, N., Price, K., Mortari, F., Alizon, M., Tsang, M. and Doms, R. W. 2001. Antigenically distinct conformations of CXCR4. *J. Virol.* **75**: 8957–8967.
2. Bendinelli, M., Pistello, M., Lombardi, S., Poli, A., Garzelli, C., Matteucci, D., Ceccherini-Nelli, L., Malvaldi, G. and Tozzini, F. 1995. Feline immunodeficiency virus: an interesting model for AIDS studies and an important cat pathogen. *Clin. Microbiol. Rev.* **8**: 87–112.
3. Berger, E. A., Murphy, P. M. and Farber, J. M. 1999. Chemokine receptors as HIV-1 coreceptors: roles in viral entry, tropism, and disease. *Annu. Rev. Immunol.* **17**: 657–700.
4. Bleul, C. C., Farzan, M., Choe, H., Parolin, C., Clark-Lewis, I., Sodroski, J. and Springer, T. A. 1996. The lymphocyte chemoattractant SDF-1 is a ligand for LESTR/fusin and blocks HIV-1 entry. *Nature* **382**: 829–833.
5. De Clercq, E. 2000. Inhibition of HIV infection by bicyclams, highly potent and specific CXCR4 antagonists. *Mol. Pharmacol.* **57**: 833–839.
6. Donzella, G. A., Schols, D., Lin, S. W., Este, J. A., Nagashima, K. A., Maddon, P. J., Allaway, G. P., Sakmar, T. P., Henson, G., De Clercq, E. and Moore, J. P. 1998. AMD3100, a small molecule inhibitor of HIV-1 entry via the CXCR4 co-receptor. *Nat. Med.* **4**: 72–77.
7. Doranz, B. J., Grovit-Ferbas, K., Sharron, M. P., Mao, S. H., Goetz, M. B., Daar, E. S., Doms, R. W. and O'Brien, W. A. 1997. A small-molecule inhibitor directed against the chemokine receptor CXCR4 prevents its use as an HIV-1 coreceptor. *J. Exp. Med.* **186**: 1395–1400.
8. Endo, Y., Goto, Y., Nishimura, Y., Mizuno, T., Watari, T., Hasegawa, A., Hohdatsu, T., Koyama, H. and Tsujimoto, H. 2000. Inhibitory effect of stromal cell derived factor-1 on the replication of divergent strains of feline immunodeficiency

virus in a feline T-lymphoid cell line. *Vet. Immunol. Immunopathol.* **74**: 303–314.
9. Hohdatsu, T., Hirabayashi, H., Motokawa, K. and Koyama, H. 1996. Comparative study of the cell tropism of feline immunodeficiency virus isolates of subtypes A, B and D classified on the basis of the env gene V3-V5 sequence. *J. Gen. Virol.* **77**: 93–100.
10. Hosie, M. J., Broere, N., Hesselgesser, J., Turner, J. D., Hoxie, J. A., Neil, J. C. and Willett, B. J. 1998. Modulation of feline immunodeficiency virus infection by stromal cell-derived factor. *J. Virol.* **72**: 2097–2104.
11. Kakinuma, S., Motokawa, K., Hohdatsu, T., Yamamoto, J. K., Koyama, H. and Hashimoto, H. 1995. Nucleotide sequence of feline immunodeficiency virus: classification of Japanese isolates into two subtypes which are distinct from non-Japanese subtypes. *J. Virol.* **69**: 3639–3646.
12. Nakashima, H., Masuda, M., Murakami, T., Koyanagi, Y., Matsumoto, A., Fujii, N. and Yamamoto, N. 1992. Anti-human immunodeficiency virus activity of a novel synthetic peptide, T22 ([Tyr-5,12, Lys-7]polyphemusin II): a possible inhibitor of virus-cell fusion. *Antimicrob. Agents Chemother.* **36**: 1249–1255.
13. Nanki, T., Hayashida, K., El-Gabalawy, H. S., Suson, S., Shi, K., Girschick, H. J., Yavuz, S. and Lipsky, P. E. 2000. Stromal cell-derived factor-1-CXC chemokine receptor 4 interactions play a central role in CD4+ T cell accumulation in rheumatoid arthritis synovium. *J. Immunol.* **165**: 6590–6598.
14. Oonuma, T., Morimatsu, M., Nakagawa, T., Uyama, R., Sasaki, N., Nakaichi, M., Tamamura, H., Fujii, N., Hashimoto, S., Yamamura, H. and Syuto, B. 2003. Role of CXCR4 and SDF-1 in mammary tumor metastasis in the cat. *J. Vet. Med. Sci.* **65**: 1069–1073.
15. Osborne, R., Rigby, M., Siebelink, K., Neil, J. C. and Jarrett. O. 1994. Virus neutralization reveals antigenic variation among feline immunodeficiency virus isolates. *J. Gen. Virol.* **75**: 3641–3645.
16. Richardson, J., Pancino, G., Merat, R., Leste-Lasserre, T., Moraillon, A., Schneider-Mergener, J., Alizon, M., Sonigo, P. and Heveker, N. 1999. Shared usage of the chemokine receptor CXCR4 by primary and laboratory-adapted strains of feline immunodeficiency virus. *J. Virol.* **73**: 3661–3671.
17. Schols, D., Este, J. A., Henson, G. and De Clercq, E. 1997. Bicyclams, a class of potent anti-HIV agents, are targeted at the HIV coreceptor fusin/CXCR-4. *Antiviral Res.* **35**: 147–156.
18. Tamamura, H., Fujisawa, M., Hiramatsu, K., Mizumoto, M., Nakashima, H., Yamamoto, N., Otaka, A. and Fujii, N. 2004. Identification of a CXCR4 antagonist, a T140 analog, as an anti-rheumatoid arthritis agent. *FEBS Lett.* **569**: 99–104.
19. Tamamura, H., Hiramatsu, K., Mizumoto, M., Ueda, S., Kusano, S., Terakubo, S., Akamatsu, M., Yamamoto, N., Trent, J. O., Wang, Z., Peiper, S. C., Nakashima, H., Otaka, A. and Fujii, N. 2003. Enhancement of the T140-based pharmacophores leads to the development of more potent and bio-stable CXCR4 antagonists. *Org. Biomol. Chem.* **1**: 3663–3669.
20. Tamamura, H., Hori, A., Kanzaki, N., Hiramatsu, K., Mizumoto, M., Nakashima, H., Yamamoto, N., Otaka, A. and Fujii, N. 2003. T140 analogs as CXCR4 antagonists identified as anti-metastatic agents in the treatment of breast cancer. *FEBS Lett.* **550**: 79–83.
21. Tamamura, H., Omagari, A., Hiramatsu, K., Gotoh, K., Kanamoto, T., Xu, Y., Kodama, E., Matsuoka, M., Hattori, T., Yamamoto, N., Nakashima, H., Otaka, A. and Fujii, N. 2001. Development of specific CXCR4 inhibitors possessing high selectivity indexes as well as complete stability in serum based on an anti-HIV peptide T140. *Bioorg. Med. Chem. Lett.* **11**: 1897–1902.
22. Trent, J. O., Wang, Z. X., Murray, J. L., Shao, W., Tamamura, H., Fujii, N. and Peiper, S. C. 2003. Lipid bilayer simulations of CXCR4 with inverse agonists and weak partial agonists. *J. Biol. Chem.* **278**: 47136–47144.
23. Willett, B. J., Picard, L., Hosie, M. J., Turner, J. D., Adema, K. and Clapham, P. R. 1997. Shared usage of the chemokine receptor CXCR4 by the feline and human immunodeficiency viruses. *J. Virol.* **71**: 6407–6415.

A New Class of Vitamin D Analogues that Induce Structural Rearrangement of the Ligand-Binding Pocket of the Receptor

Yuka Inaba,[†,‡] Nobuko Yoshimoto,[†] Yuta Sakamaki,[†,§] Makoto Nakabayashi,[‡,§] Teikichi Ikura,[‡] Hirokazu Tamamura,[§] Nobutoshi Ito,[‡] Masato Shimizu,[‡,§] and Keiko Yamamoto*[,†]

Laboratory of Drug Design and Medicinal Chemistry, Showa Pharmaceutical University, 3-3165 Higashi-Tamagawagakuen, Machida, Tokyo 194-8543, Japan, School of Biomedical Science, Institute of Biomaterials and Bioengineering, Tokyo Medical and Dental University, 2-3-10 Kanda-Surugadai, Chiyoda-ku, Tokyo 101-0062, Japan

Received November 13, 2008

To identify novel vitamin D receptor (VDR) ligands that induce a novel architecture within the ligand-binding pocket (LBP), we have investigated eight 22-butyl-1α,24-dihydroxyvitamin D_3 derivatives (**3**–**10**), all having a butyl group as the branched alkyl side chain. We found that the 22*S*-butyl-20-epi-25,26,27-trinorvitamin D derivative **5** was a potent VDR agonist, whereas the corresponding compound **4** with the natural configuration at C(20) was a potent VDR antagonist. Analogues with the full vitamin D_3 side chain were less potent agonist, and whether they were agonists or antagonists depended on the 24-configuration. X-ray crystal structures demonstrated that the VDR-LBD accommodating the potent agonist **5** has an architecture wherein the lower side and the helix 11 side of the LBP is simply expanded relative to the canonical active-VDR situation; in contrast, the potent antagonist **4** induces an extra cavity to accommodate the branched moiety. This is the first report of a VDR antagonist that generates a new cavity to alter the canonical pocket structure of the ligand occupied VDR.

Introduction

The hormonally active metabolite of vitamin D_3, 1α,25-dihydroxyvitamin D_3 [1,25-$(OH)_2D_3$, **1a**], plays an important role in calcium homeostasis, cell differentiation and proliferation, and immunomodulation.[1] 1,25-$(OH)_2D_3$ (**1a**) and its active analogues exert these effects by binding to the vitamin D receptor (VDR[a]), which belongs to the nuclear receptor superfamily.[2] The VDR is a ligand-dependent transcription factor that functions as a heterodimer with another nuclear receptor, retinoid X receptor (RXR).[3] Upon ligand binding, the VDR undergoes a conformational change that promotes RXR–VDR heterodimerization.[3] The RXR–VDR heterodimer binds to the vitamin D response elements present in the promoter region of responsive genes, recruits the coactivator, and initiates the transcription.

Since the first report of the X-ray crystal structure of the ligand binding domain (LBD) of the VDR complexed with the hormone 1,25-$(OH)_2D_3$ (**1a**) by Moras' group in 2000,[4] several groups have solved the crystal structures of the VDR–LBD complexed with a variety of ligands.[5–16] All of the crystal structures showed the canonical Moras' conformation of the VDR–LBD and quite similar architectures of the ligand binding pocket (LBP), except for the complex of zebrafish VDR–LBD with "GEMINI, **1b**",[7,11] an analogue with two identical side chains.[17,18] The zebrafish VDR–LBD/GEMINI complex revealed the formation of a new channel extending the original LBP in order to accommodate the second side chain. This particular observation suggests that the region around helix 6, the subsequent loop 6–7, and the N-terminal of helix 7 has a certain flexibility without loss of function because, despite the new pocket structure, GEMINI **1b** acts as a VDR agonist.[19] We considered that some new ligands having the right side chain might be able to change the induced pocket structure in such a way as to modulate the VDR differently. Here, we report a novel class of vitamin D analogues exhibiting a stereospecific dichotomy of activities.

Design and Synthesis

We have already reported that some 22-alkyl-1α,25-dihydroxyvitamin D_3, and in particular the 20-epi analogues, act as superagonists of the VDR.[20–22] Docking analysis and alanine scanning mutational analysis (ASMA) gave a clue that the 22-alkyl substituent of 22*R*-butyl-20-epi-1,25-$(OH)_2D_3$ **2** might induce a novel cavity in a similar way to GEMINI **1b**.[22] To explore further vitamin D compounds possessing a 22-butyl group, we have now investigated a series of 22-butyl-1α,24-dihydroxyvitamin D_3 derivatives **3**–**10** as candidate VDR modulators. The 25-to-24 transposition of the hydroxyl group is a known agonistic modification, notably seen in several clinically important vitamin D analogues. In compounds **3**–**6**, three carbons at the side chain terminus were removed to decrease the degree of hydrophobic interactions with helix 12, including the terminal of helix 11, of the VDR. On the basis of our previous study, we had concluded that insufficient hydrophobic interactions between the ligand and the C-terminal of the VDR cause antagonistic behavior.[23] Compounds **7**–**10** were designed as the counterparts of side chain truncated analogues **3** and **4** to test the significance of the hydrophobic interactions (Chart 1).

As shown in Scheme 1, 22-butyl vitamin D derivatives **3** and **4** were synthesized from 22*R*-butyl compound **11** and 22*S*-butyl compound **12**, respectively, which are the established products of a diastereofacial selective conjugate addition reaction of *n*-Bu_2CuLi with the *E*- and *Z*-enoates developed by our group previously.[24] The configuration at C(22) follows from the

* To whom correspondence should be addressed. Phone: +81 42 721 1580. Fax: +81 42 721 1580. E-mail: yamamoto@ac.shoyaku.ac.jp.

† Laboratory of Drug Design and Medicinal Chemistry, Showa Pharmaceutical University.

‡ School of Biomedical Science, Tokyo Medical and Dental University.

§ Institute of Biomaterials and Bioengineering, Tokyo Medical and Dental University.

[a] Abbreviations: VDR, vitamin D receptor; LBP, ligand binding pocket; 1,25-$(OH)_2D_3$, 1α,25-dihydroxyvitamin D_3; RXR, retinoid X receptor; LBD, ligand binding domain; ASMA, alanine scanning mutational analysis.

10.1021/jm8014348 CCC: $40.75
Published on Web 02/04/2009

Chart 1. Structures of 1,25-$(OH)_2D_3$ (**1a**) and Its Derivatives

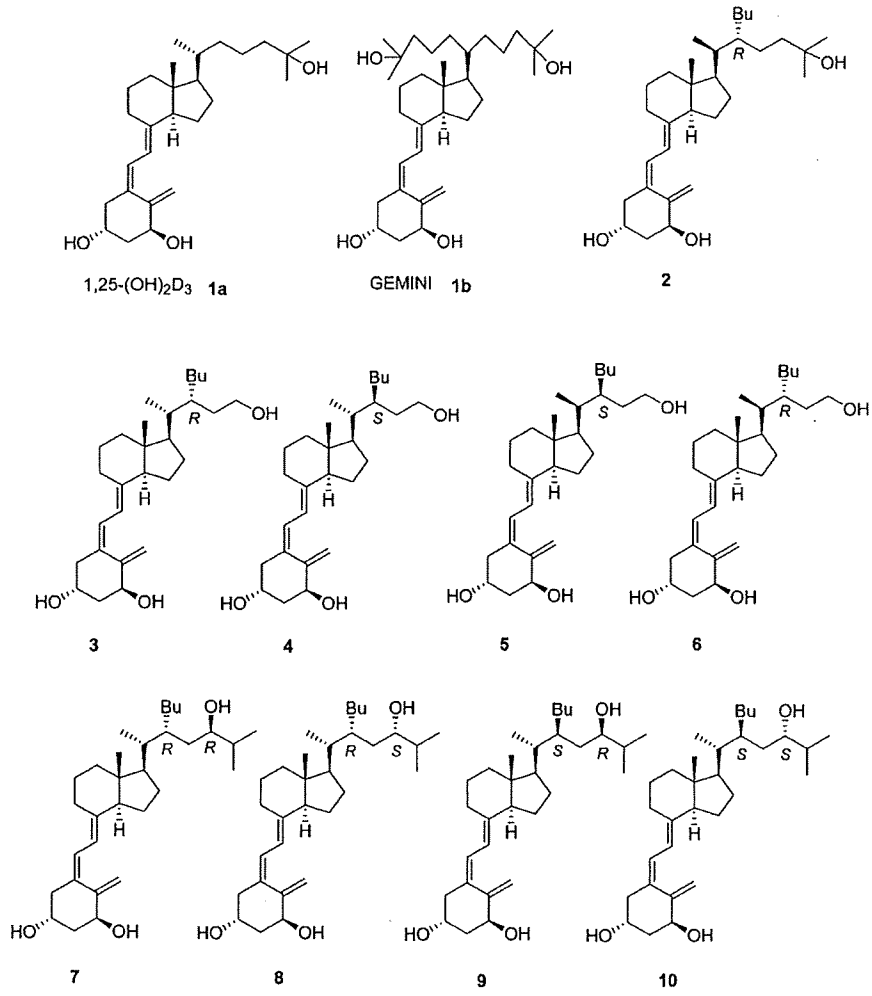

stereochemistry of the starting enoates and the reaction conditions.[24] Reduction of the side chain ester together with reductive cleavage of the carbonates at C(1) and C(3) as protecting groups of **11** and **12** gave provitamins D, **13** and **14**, respectively. These provitamins were converted to the desired vitamin D analogues **3** and **4** by the biomimetic sequence of photoirradiation with a high-pressure mercury lamp, followed by thermal isomerization. The 20-epi-analogues **5** and **6** were synthesized by the analogous procedure as that described above for the synthesis of the 20-normal analogues **3** and **4**.

22-Butyl-1α,24-dihydroxyvitamins D_3 **7**−**10** were successfully synthesized from the same 22-butyl compounds **11** and **12**. Controlled chemoselective reduction of the methyl esters of **11** and **12** by DIBAL afforded 24-alcohols **19** and **20**, respectively. Swern oxidation of the 24-alcohols **19** and **20** gave the aldehyde **21** and **22**, respectively. 22*R*-aldehyde **21** reacted with *i*-PrMgCl to give the 24*R*- and 24*S*-isomers **23** (less polar) and **24** (more polar), while 22*S*-aldehyde **22** reacted with *i*-PrMgCl to give the 24*R*- and 24*S*-isomers **25** (less polar) and **26** (more polar). Epimers were separated by column chromatography. The configuration at C24 was determined by the Kusumi−Mosher method (Scheme 2).[25] Thus, less polar compound **23** was converted to the corresponding *S*- and *R*-MTPA esters of the 24-hydroxyl group (**31** and **32**), and the 22-isomer **26** was also converted to those of the 24-hydroxyl group (**33** and **34**). Chemical shift differences between the *S*-MTPA ester and the corresponding *R*-MTPA ester are shown in Figure 1a,b. This analysis clearly indicated that the 24-alcohols **23** and **26** have a 24*R*-configuration and a 24*S*-configuration, respectively. Consequently, the configurations of 24-isomers **24** and **25** were demonstrated to be *S* and *R*, respectively. Methyl carbonates at C(1) and C(3) were saponified to give provitamins D **27**−**30**. These provitamins were converted to the desired vitamin D analogues **7**−**10** by photoirradiation, followed by thermal isomerization.

Biological Activities

Binding affinity for the VDR was evaluated by the standard competitive binding assay using bovine thymus VDR, which has a LBD amino acid sequence[26] identical to that of the human VDR.[27] The results are summarized in Table 1. Of the four 22-butyl-1α,24-dihydroxy-25,26,27-trinorvitamins D_3 **3**−**6**, the 22*S*-compounds **4** and **5** showed significant affinity compared to the natural hormone **1a**, while their 22*R*-isomers **3** and **6** showed weak affinity for the VDR. Among the four 22-butyl-1α,24-dihydroxyvitamins D_3 **7**−**10**, both of the 24*S*-hydroxyl compounds **8** and **10** showed significant affinity for the VDR, while both the 24*R*-hydroxyl compounds **7** and **9** showed relatively weak affinity.

The ability of 22-butyl compounds **3**−**10** to induce transcription of a vitamin D-responsive gene was tested using the rat osteopontin luciferase reporter gene assay system in Cos7 cells, and the results are shown in Figure 2. In this assay, only

Scheme 1. Synthetic Sequence Leading to Target Compounds **3**–**10**

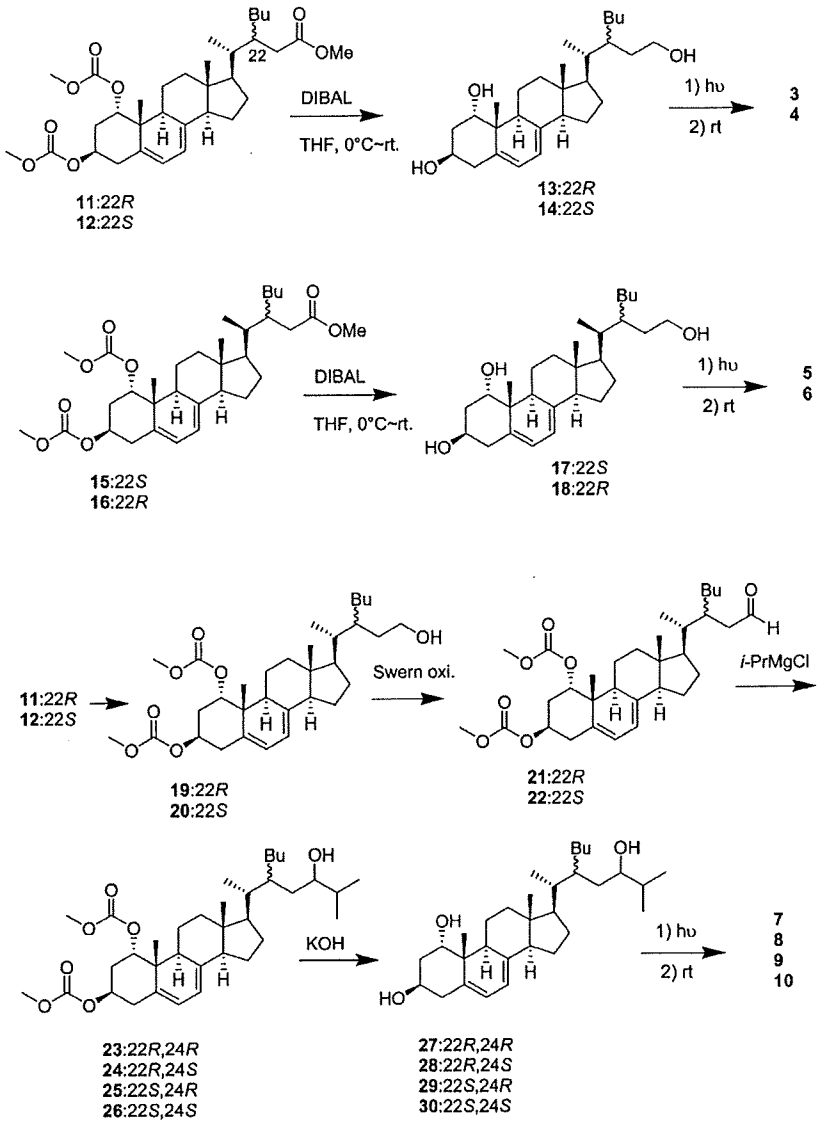

Scheme 2. MTPA esters from 24-Alcohols **23** and **26**

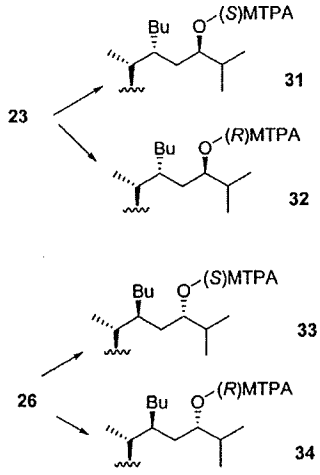

compound **5** showed full agonistic activity and two analogues **7** and **9** showed weak agonist activity. All of the others, **3**, **4**, **6**, **8**, and **10**, showed little activity. It is known that receptor affinity and transactivation potency are not proportional to each other.[22,28] The potency to inhibit VDR activation was evaluated in the presence of 1 nM 1,25-$(OH)_2D_3$ (**1a**). As shown in Figure 2, compounds **4**, **6**, **8**, and **10** concentration-dependently inhibited the transactivation induced by 1,25-$(OH)_2D_3$ (**1a**), indicating that these four analogues work as VDR antagonists. We performed the same assays in HEK293 cells and obtained similar results (see Supporting Information Figure S1).

We evaluated the expression of CYP24A1 mRNA in HEK293 cells by quantitative real-time PCR. CYP24A1 is known to be the most potent target gene of the hormone 1,25-$(OH)_2D_3$ (**1**).[29a] In accordance with the transcriptional activities of our synthetic ligands described above, only compound **5** expressed CYP24A1 mRNA strongly in comparison with the natural hormone **1a**, and compound **9** showed weak expression activity (Figure 3a,b). All of the others, **3**, **4**, **6**, **7**, **8**, and **10**, showed little activity. The inhibition potency of synthetic ligands for CYP24A1 mRNA expression was evaluated in the presence of 10 nM 1,25-$(OH)_2D_3$ (**1a**). As shown in Figure 3a,b, compounds **4**, **6**, **8**, and **10** significantly inhibited the gene expression induced by 1,25-$(OH)_2D_3$ (**1a**). Figure 3c shows that compound **4** inhibited the gene expression concentration-dependently.

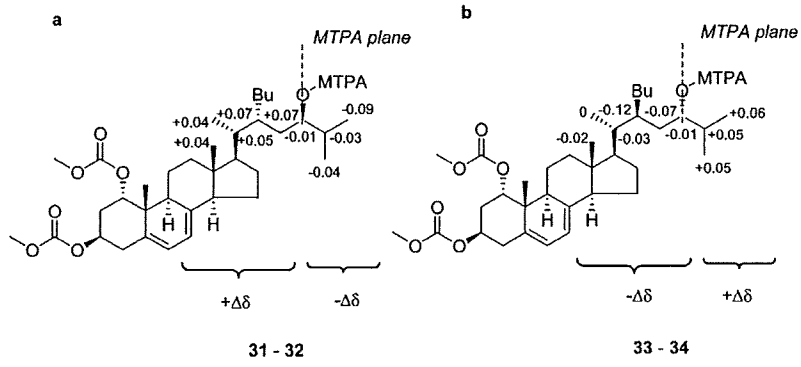

Figure 1. Determination of stereochemistry at C(24). Chemical shift differences.

Table 1. VDR Binding Affinity of 22-Butyl Compounds **3**−**10**[a]

	1a	**3** (22*R*)	**4** (22*S*)	**5** (22*S*)	**6** (22*R*)	**7** (22*R*,24*R*)	**8** (22*R*,24*S*)	**9** (22*S*,24*R*)	**10** (22*S*,24*S*)
EC_{50} (nM)[b]	0.05	11	1.2	2.0	20	16	3.4	20	3.8
relative affinity[c]	1	1/220	1/24	1/40	1/400	1/320	1/68	1/400	1/76

[a] Competitive binding of 1,25-$(OH)_2D_3$ (**1a**) and 22-butyl compounds (**3**−**10**) to the bovine thymus vitamin D receptor. The experiments were carried out in duplicate. [b] The EC_{50} values are derived from dose−response curves and represent the compound concentration required for 50% displacement of the radio-labeled 1,25-$(OH)_2D_3$ from the receptor protein. [c] Affinity relative to 1,25-$(OH)_2D_3$ (**1a**), the activity of **1a** being defined as 1.

Cell differentiation and antiproliferation activity were evaluated using human promyelocyte HL-60 cells.[29b] Compound **5** showed significant activity for differentiation of HL-60 cells into monocytes/macrophages (Figure 4), being comparable to that of 1,25-$(OH)_2D_3$ (**1a**), whereas compound **9** showed weak activity. None of the other compounds induced differentiation of HL-60 cells. Similar results were obtained in experiments examining the antiproliferative effect on HL-60 cells (data not shown). Ligand **4** concentration-dependently inhibited the differentiation and antiproliferation of HL-60 cells induced by stimulation with 1,25-$(OH)_2D_3$ (**1a**) (Figure 4c). Morphologic analysis also indicated that the differentiation of HL-60 cells was inhibited by ligand **4** (Figure 4d).

Thus, in all assays, ligands **4** and **5** were demonstrated to behave as a potent antagonist and a potent agonist, respectively.

Alanine Scanning Mutational Analysis

We have developed and reported a method for exhaustive alanine scanning mutational analysis (ASMA) of residues lining the LBP of the VDR.[30] We applied this analysis to all eight compounds **3**−**10**. Transactivation was examined using 22-butyl compounds (**3**−**10**) at a concentration of 10^{-6} M. The results are shown in Figure S2 (see Supporting Information) in comparison with the natural hormone (**1a**) and the parent molecule, 22*R*-butyl-20-epi-1,25-$(OH)_2D_3$ **2**.

Recruitment of RXR and Coactivator Peptide

We evaluated ligand-dependent recruitment of the RXR and a coactivator peptide, SRC-1, to the VDR using a mammalian two-hybrid assay similar to that reported previously.[31] As shown in Figure S3 of the Supporting Information, compound **5** recruited the RXR and SRC-1 strongly, whereas compounds **7** and **9** did so weakly. Inhibition of SRC-1 recruitment induced by natural hormone **1a** was observed for compounds **4**, **8**, and **10** (data not shown).

Structure

To understand the molecular basis of action of our synthetic ligands, we conducted X-ray crystal structure analysis of the VDR−LBD/ligand complex and successfully solved the crystal structure of rat VDR−LBD bound to the potent agonist **5** in the presence of the coactivator peptide at 2.1 Å resolution (Table 2). A ribbon-tube representation of the rVDR−LBD/**5**/peptide complex is shown in Figure 5a, and the results of the crystallographic refinement are summarized in Table 2. The electron density of the VDR−LBD complex including ligand **5** is well defined. The overall structure of the VDR−LBD is similar to that observed for VDR−LBD bound to 1,25-$(OH)_2D_3$ (**1a**),[15] although the ligand **5** has a branched alkyl side chain. The coactivator peptide is tightly bound to the activation function 2 surface formed by helices 3, 4, and 12 of the LBD and occupies the typical agonist position (Figure 5a). However, the docking mode of agonist **5** is unusual. In the crystal structure, the part from the A-ring to the D-ring occupies almost the same position as that of 1,25-$(OH)_2D_3$ (**1a**), but the mode in which the side chain is accommodated into the pocket is unique (Figure 5b), i.e., the 22-butyl group, and not the canonical side chain bearing the 24-hydroxyl group, is oriented toward helix 12, and the 24-hydroxyl group itself is oriented toward helix 6 to form a hydrogen bond with the carbonyl oxygen of the main chain of Val296 (hVal300) on helix 6. Because both of the side chains of ligand **5** are accommodated tightly in the pocket of the VDR active conformation, the pocket is slightly expanded in the bottom (lower) region, where the side chain hydroxyl group of **5** is located, and in the terminal region of helix 11, where the terminal of the butyl group of **5** is located together with a molecule. The expansion of the bottom region results from steric repulsion between the side chains of the residues on helix 6 and the subsequent loop 6−7 of the VDR and the 24-hydroxyl group of ligand **5**. Expansion at the helix 11 side is caused by twisting of the side chain of Leu400 (hLeu404) on loop 11−12 (Figure 5b).

To understand the structural basis of the antagonistic effect of compound **4**, we attempted to solve the crystal structure of the VDR−LBD/**4** complex. We were able to obtain crystals of the complex in the presence of the coactivator peptide, but not in its absence. The resolution of the ternary complex (rVDR−LBD/**4**/peptide) was 3.0 Å (Table 2). The electron density of the main chain of the VDR−LBD and almost all of ligand **4** was clearly observed. The overall structure of the main chain, including helices 11 and 12, is quite similar to that of the VDR−LBD/**1a**/peptide complex (Figure 6a). The main chains of only two

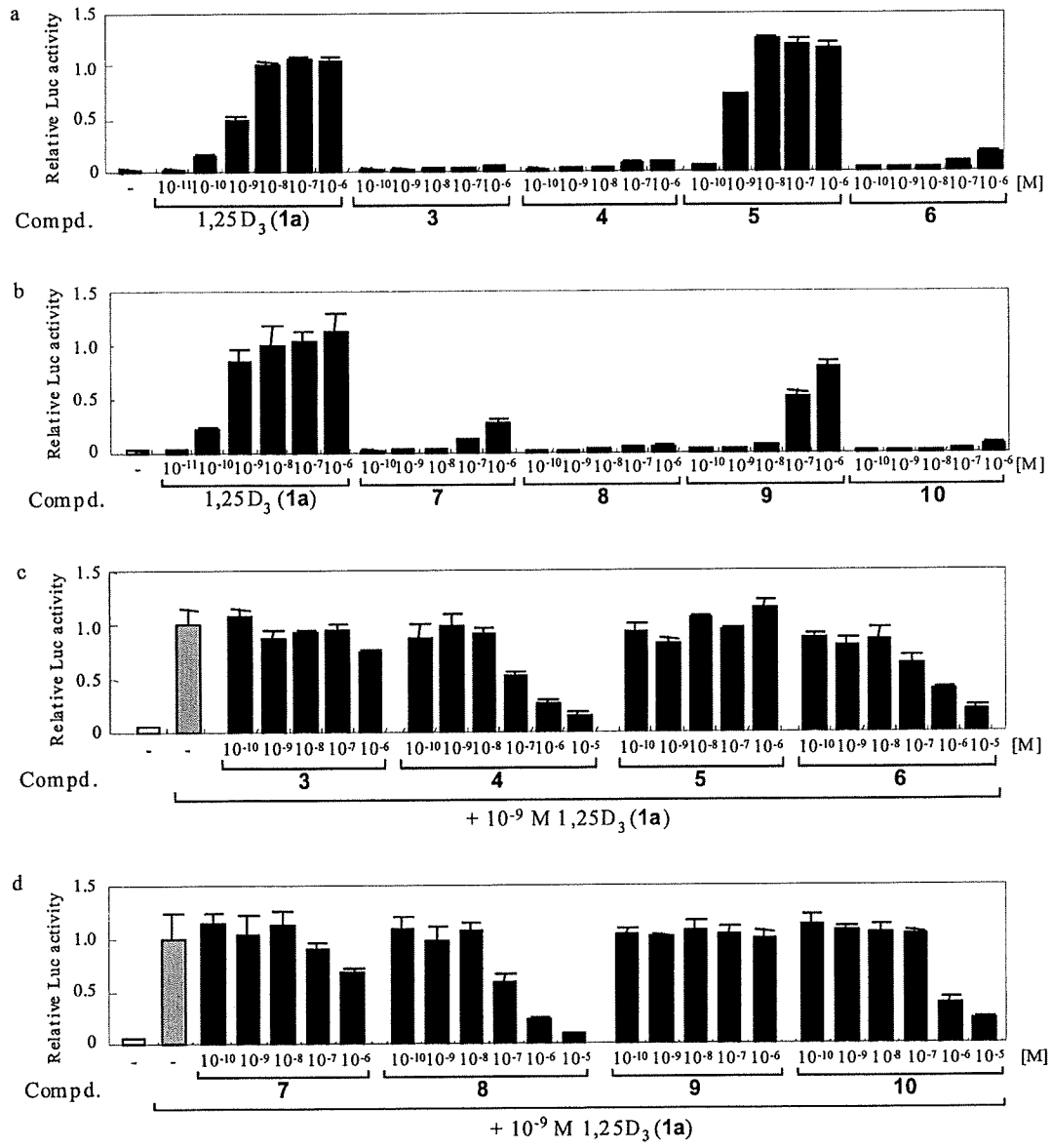

Figure 2. Transactivation of compounds **3**−**10** in Cos7 cells. Transcriptional activity (a and b) and inhibitory effect on the transactivation induced by 1,25-$(OH)_2D_3$ (**1a**) (c and d) were evaluated by dual luciferase assay using a full-length human VDR expression plasmid (pCMX-hVDR), a reporter plasmid containing three copies of the mouse osteopontin VDRE (SPPx3-TK-Luc), and the internal control plasmid containing sea pansy luciferase expression constructs (pRL-CMV) in Cos7 cells as described previously.[32] Luciferase activity in the presence of 10^{-8} M 1,25-$(OH)_2D_3$ (**1a**) was defined as 1: (a) transcriptional activity of **1a** and **3**−**6**, (b) transcriptional activity of **1a** and **7**−**10**, (c) transcriptional activity of **3**−**6** in the presence of 10^{-9} M 1,25-$(OH)_2D_3$ (**1a**), (d) transcriptional activity of **7**−**10** in the presence of 10^{-9} M 1,25-$(OH)_2D_3$ (**1a**). All experiments were done in triplicate.

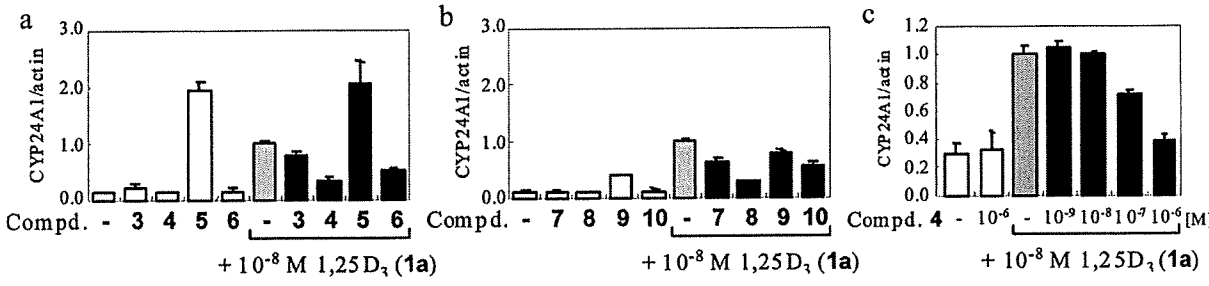

Figure 3. Effect of **1a** and 22-butyl compounds (**3**−**10**) on expression of the CYP24A1 gene in HEK293 cells. (a,b) Cells were treated with 10^{-6} M 22-butyl compounds ((a) **3**−**6**, (b) **7**−**10**) in the absence or presence of 10^{-8} M 1,25-$(OH)_2D_3$ (**1a**) for 24 h. Concentration (10^{-6} M) of test compounds was selected to obtain clear results concerning whether they activate CYP24A1 expression or inhibit it. (c) Cells were treated with the indicated concentrations of compounds for 24 h. All experiments were carried out in triplicate.

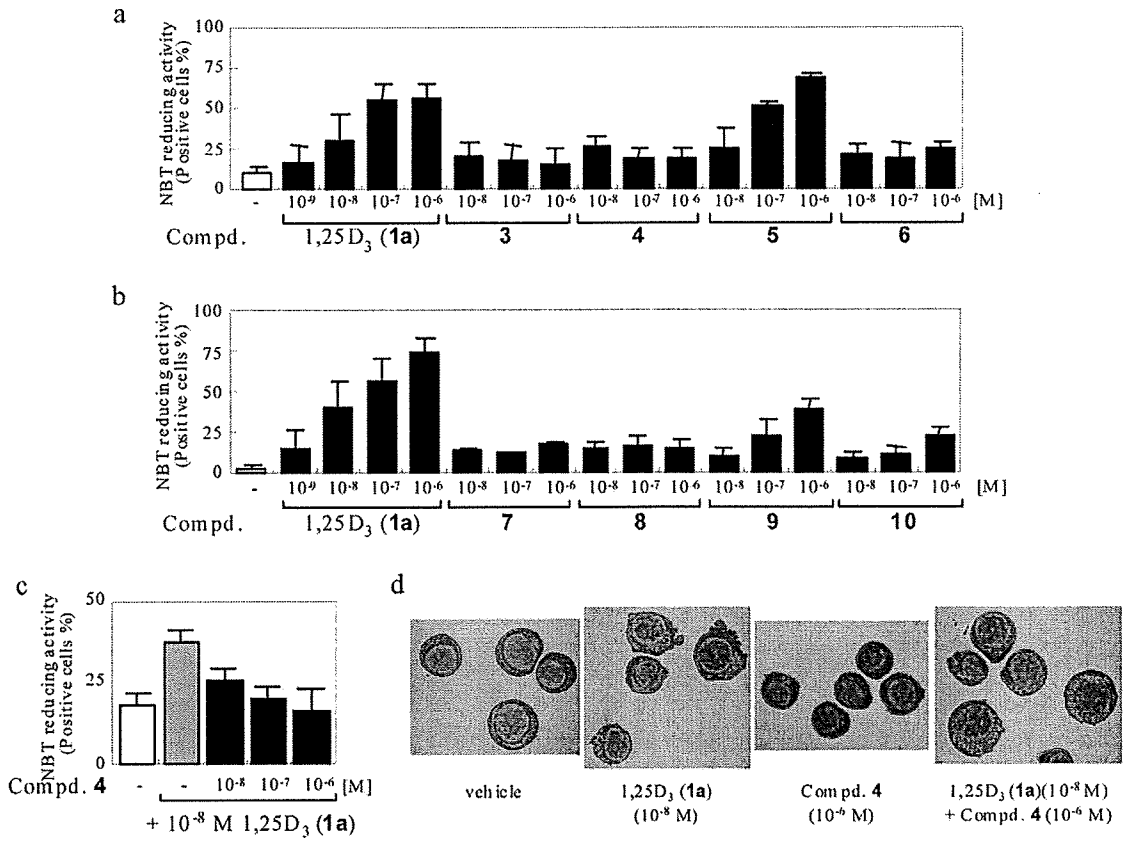

Figure 4. Effect of **1a** and 22-butyl compounds (**3**−**10**) on differentiation of HL-60 cells. (a−c) Cells were treated with the indicated concentrations of compounds for four days. Differentiation was determined by nitro blue tetrazolium (NBT) reduction.[33] All experiments were carried out in triplicate. (d) HL-60 cells were stained with Wright−Giemsa and analyzed for morphology by light microscopy.

Table 2. Summary of Data Collection Statistics and Refinement

ligand	compd **4**	compd **5**
X-ray source	KEK-PF BL-6A	KEK-PF BL-6A
wavelength (Å)	0.97800	0.97800
space group	*C*2	*C*2
unit cell dimensions (Å)	a = 153.25, b = 43.42, c = 42.37	a = 153.16, b = 43.88, c = 41.89
(deg)	α = 90.00, β = 95.97, γ = 90.00	α = 90.00, β = 95.89, γ = 90.00
resolution range (Å)[a]	50.00−3.00 (3.11−3.00)	50.00−2.10 (2.18−2.10)
total number of reflections	17932	59861
no. of unique reflections	5664	16470
% completeness[a]	99.1 (99.8)	97.5 (92.2)
R_{merge}[a,b]	0.086 (0.392)	0.045 (0.234)
refinement statistics		
resolution range (Å)[a]	50.00−3.00 (3.11−3.00)	50.00−2.10 (2.18−2.10)
R factor (R_{free}/R_{work})[a,c]	0.295 (0.431)/0.226 (0.321)	0.251 (0.367)/0.209 (0.336)

[a] Values in parentheses are for the highest-resolution shell. [b] $R_{merge} = \Sigma|(I_{hkl} - \langle I_{hkl}\rangle)|/(\Sigma I_{hkl})$, where $\langle I_{hkl}\rangle$ is the mean intensity of all reflections equivalent to reflection hkl. [c] R_{work} (R_{free}) = $\Sigma||F_{obs}| - |F_{calc}||/\Sigma|F_{obs}|$, where 10% of randomly selected data were used for R_{free}.

amino acid residues, Leu305 (hLeu309) and Ser394 (hSer398), are slightly twisted outward (Figure 6b). The crystal structure clearly demonstrated that a novel cavity is produced in the region surrounded by helix 6, the subsequent loop 6−7, the N-terminal of helix 7 and helix 11, as in the zVDR/GEMINI complex, because the terminal of the 22-butyl group of **4** pushes out the side chain of Leu305 to rearrange the LBP (Figure 6c,d).

Thus, we identified a new class of VDR ligands with a simple side chain that modulate the structure of the LBP.

Discussion

Compound **5** was proved to have potent agonistic activity by additional experiments involving RXR recruitment and SRC-1 peptide recruitment using a mammalian two-hybrid assay (see Supporting Information Figure S3). These experimental results corroborate the crystal structure of the VDR−LBD/**5**/peptide complex (Figure 5). Thus, the overall surface structure is rather similar to that of the VDR−LBD/**1a**/peptide complex. On the other hand, ligand **5** is accommodated into the LBP by an unusual docking mode in which two side chains of ligand **5**, together with a molecule, increase the volume of the LBP. The pocket is filled sufficiently with ligand **5** and a water molecule. These observations well account for the potent activity of compound **5**.

The antagonistic activity of compound **4** was also confirmed by experiments involving RXR recruitment and SRC-1 peptide recruitment (see Supporting Information Figure S3). So far, the X-ray crystal structure of the VDR−LBD/antagonist complex, which clearly explains the structural basis of the antagonism,

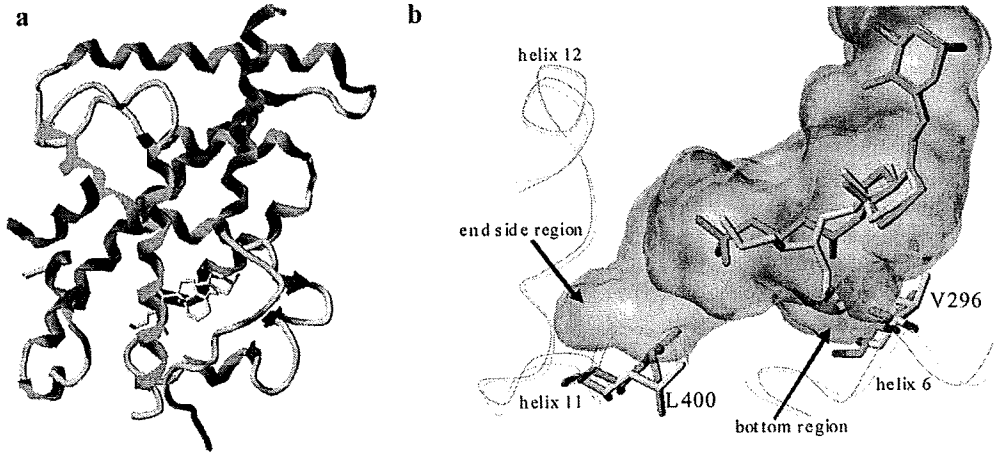

Figure 5. X-ray crystal structure of rVDR−LBD/**5**/peptide complex. (a) Overall view of rVDR−LBD/**5**/peptide complex. Helices, loops, β-sheets, and coactivator peptide are shown in green, yellow, violet, and red, respectively. Ligand **5** is shown in gray with the oxygen atoms in red. (b) Superposition of rVDR−LBD/**1a**/peptide (green) and rVDR−LBD/**5**/peptide (pink) in the ligand binding pocket (LBP) region. Connolly channel surfaces of the LBP of rVDR−LBD/**1a**/peptide and rVDR−LBD/**5**/peptide are shown in green and pink, respectively. Hydrogen bond is shown with dotted orange line. Water molecule is shown in red sphere.

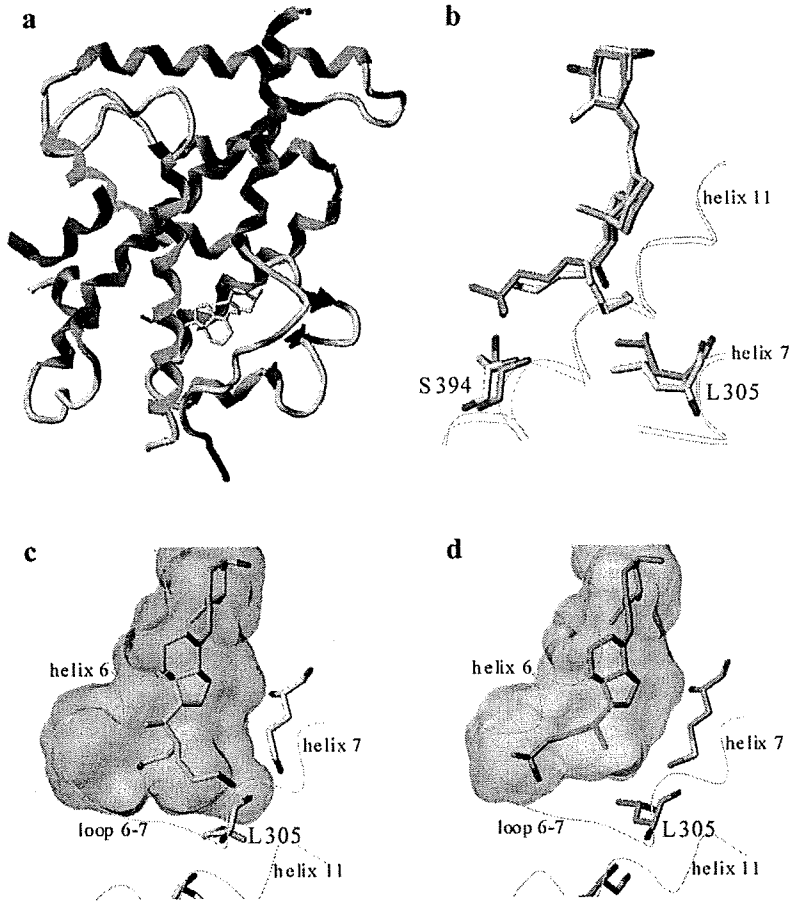

Figure 6. X-ray crystal structure of rVDR−LBD/**4**/peptide complex. (a) Overall view of rVDR−LBD/**4**/peptide complex. Helices, loops, β-sheets, and coactivator peptide are shown in green, yellow, violet, and red, respectively. The ligand **4** is shown in gray with the oxygen atoms in red. (b) Superposition of rVDR−LBD/**1a**/peptide (green) and rVDR−LBD/**4**/peptide (gray) in the ligand biding pocket (LBP) region. (c) Connolly channel surface of the LBP of rVDR−LBD/**4**/peptide. (d) Connolly channel surface of the LBP of rVDR−LBD/**1a**/peptide.

has not been reported. Quite recently, the crystal structure of the VDR−LBD complex accommodating an antagonist with a coactivator peptide was reported, where the ligand was bound to the active (agonistic) conformation of the VDR.[16] This situation was also the case in the present study. We were able to obtain crystals of the VDR−LBD/**4** complex in the presence of, but not in the absence of, the coactivator peptide as a ternary complex (Figure 6). Considering the action of compound **4** as a VDR antagonist, the active (agonistic) conformation of the VDR−LBD/**4** complex bound tightly to the peptide seems to be a temporary and less preferred structure but selected in the course of crystallization. This idea is consistent with the fact

that the resolution limit of this crystal (3.0 Å) is much lower than that of the crystal for compound **5** (2.1 Å). Therefore, the active conformation observed in our crystal structure may not exactly correspond to the predominant one in vivo. Meanwhile, it is true that ligand **4** modifies the pocket structure to induce a new cavity, as seen in the zVDR−LBD/GEMINI complex.[11] Unlike GEMINI, however, compound **4** showed antagonistic activity. This discrimination can be explained mainly by the difference in hydrophobic interactions between the side chain terminals of the ligand and the C-terminal of the VDR. This explanation agrees with the fact that compound **9**, which restored the three truncated carbons on the side chain, restored the agonistic activity, albeit weakly.

Compound **6**, which is 25,26,27-trinor analogue of the previously reported 22*R*-butyl-20-epi-1,25-$(OH)_2D_3$ **2**, having potent agonistic activity,[22] showed weak VDR affinity and little agonistic or antagonistic activity. ASMA of compound **6** yielded results similar to those for 22*R*-butyl-20-epi-1,25-$(OH)_2D_3$ **2**, indicating that **6** is accommodated into the VDR−LBD by the similar docking mode to that of the parent compound **2**. However, interaction of a hydrogen bond with His397 is not important for **6** because H397A did not decrease the transcriptional activity in comparison with the wild type. In addition, compound **6** lacks the intimate hydrophobic interactions with the C-terminal residues of the VDR because of truncation of the three carbons in the side chain terminal. Therefore, the weak activity of ligand **6** is attributable to poor interaction with the C-terminal regions (helix 11-helix 12) of the VDR.

Docking analysis of ligand **8** into the crystal structure of the VDR−LBD/**4**/peptide complex demonstrated that the two side chains of ligand **8** occupy opposite cavities, respectively, (data not shown) in comparison with the VDR−LBD/**4** complex. This mode is consistent with the results of ASMA. The increased activity of H397A and H305A compared with the wild type (Supporting Information Figure S2h) suggests that His397 does not form an important hydrogen bond with ligand **8** and His305 exhibits crucial steric repulsion from the ligand.

Docking analysis of ligand **10** demonstrated that its mode of docking into the LBP is similar to that of compound **4**. When taking together with the results of ASMA, it appears that steric repulsion between the *i*-propyl group of the side chain terminal of **10** and the side chain of His305 explains the antagonistic activity.

GEMINI (**1b**), which has two identical side chains branching at C(20), induces structural rearrangement of the LBP.[11] We identified potent agonist **5** and potent antagonist **4**, both of which have a branched 22*S*-butyl group and are isomers at C(20). We found that both ligands rearrange the pocket structure of the VDR through an unusual docking mode that has not yet been reported. Other ligands (**3**, **6**−**10**) showed intermediate activities (weakly agonistic and weakly antagonistic) and appeared to modify the LBP structure moderately. It is interesting that although GEMINI (**1b**) and our compound **4** are accommodated into the VDR−LBD through a similar docking mode, GEMINI (**1b**) works as a VDR agonist whereas compound **4** works as a VDR antagonist.

Conclusions

We synthesized 22-butyl-1,24-$(OH)_2D_3$ derivatives **3**−**10** and evaluated their biological activities. Four compounds, **4**, **5**, **8**, and **10**, showed significant VDR binding affinity but three of them, **4**, **8**, and **10**, showed little transactivation, cell differentiation, and CYP24A1 gene expression potency. Instead, these three compounds concentration-dependently inhibited biological activities induced by 1,25-$(OH)_2D_3$, indicating that they are VDR antagonists. On the basis of X-ray crystallographic analysis, we identified a new class of ligands that modulate the pocket structure of the VDR. This is the first report of a VDR antagonist that generates a new cavity to alter the pocket structure of the VDR, opening an interesting new perspective of ligand design based on the alternative structural basis of VDR agonism and antagonism.

Experimental Section

^1H NMR and ^{13}C NMR spectra were recorded in $CDCl_3$ at 400 MHz, and chemical shifts are reported as δ units relative to tetramethylsilane as an internal standard. High and low resolution mass spectra were obtained at 70 eV. Relative intensities are given in parentheses in low mass. IR spectra were recorded on a Shimazu FTIR spectrometer. UV spectra were recorded on a BECKMAN DU7500 spectrophotometer. All air and moisture sensitive reactions were carried out under argon atmosphere.

22*R*-Butyl-(1α,3β)-chola-5,7-diene-1,3,24-triol (13). To a solution of **11** (50 mg, 0.087 mmol) in THF (1 mL) was added diisobutyl-alminum hydride (DIBAL, 1.0 M solution in toluene, 1000 μL, 1 mmol) at 0 °C and the mixture was stirred for 2.5 h. Then the mixture was allowed to come to room temperature and was stirred for 10 h. The reaction mixture was poured into ice−water, extracted with ethyl acetate, washed with water, dried over Na_2SO_4, and evaporated. The residue was chromatographed on silica gel (C-200, 4 g) with 3% EtOH−CH_2Cl_2 to give **13** (24 mg, 64%). ^1H NMR δ 0.64 (3 H, s, H-18), 0.81 (3 H, d, J = 6.9 Hz, H-21), 0.90 (3 H, t, J = 6.4 Hz, CH_3 of *n*-Bu), 0.95 (3 H, s, H-19), 3.58 and 3.71 (each 1 H, m, H-24), 3.77 (1 H, m, H-1), 4.08 (1 H, m, H-3), 5.38 and 5.74 (each 1 H, m, H-6 and H-7). MS *m*/*z* 430 (M^+, 10), 412 (6), 394 (11), 371 (13), 55 (100). UV (EtOH) λ_{max} 272, 282, 294 nm.

22*S*-Butyl-(1α,3β)-chola-5,7-diene-1,3,24-triol (14). The compound **14** was obtained from **12** (0.35 mmol) by the same procedure as described for **13** (yield 75%). ^1H NMR δ 0.63 (3 H, s, H-18), 0.83 (3 H, d, J = 6.1 Hz, H-21), 0.90 (3 H, t, J = 6.7 Hz, CH_3 of Bu), 0.95 (3 H, s, H-19), 3.62 and 3.68 (each 1 H, m, H-24), 3.77 (1 H, m, H-1), 4.07 (1 H, m, H-3), 5.38 and 5.74 (each 1 H, m, H-6 and H-7). MS *m*/*z* 430 (M^+, 14), 412 (8), 394 (15), 371 (20), 55 (100). UV (EtOH) λ_{max} 272, 282, 294 nm.

22*R*-Butyl-1α,24-dihydroxy-24,25,26-trinorvitamin D_3 (3). A solution of provitamin D **13** (22 mg, 0.051 mmol) in benzene/EtOH (130:50, 180 mL) was bubbled with argon at 0 °C for 15 min and then irradiated with a 100 W high pressure mercury lamp through a Vycor filter until most of the starting material **13** was consumed. After removal of the solvent, the residue was chromatographed on Sephadex LH-20 (15 g) with $CHCl_3$/hexane/MeOH (70:30:1.5) to give previtamin D. The previtamin D in 95% EtOH (5 mL) was stored in the dark at room temperature. After 12 days, the solution was evaporated and the residue was chromatographed on Sephadex LH-20 (15 g) with $CHCl_3$/hexane/MeOH (70:30:2) to give desired vitamin D **3** (5.0 mg, 23%). The purity was proved to be more than 99% by two different HPLC systems: (1) YMC Pack ODS-AM 4.6 mm × 150 mm, H_2O/MeOH (15:85), 1.0 mL/min; (2) PEGASIL Silica SP100, 4.6 mm × 150 mm, hexane/$CHCl_3$/MeOH (100:25:10), 1.0 mL/min. ^1H NMR δ 0.56 (3 H, s, H-18), 0.79 (3 H, d, J = 6.7 Hz, H-21), 0.89 (3 H, t, J = 6.7 Hz, CH_3 of *n*-Bu), 3.58 and 3.72 (each 1 H, m, H-24), 4.23 (1 H, m, H-3), 4.43 (1 H, m, H-1), 5.00 and 5.33 (each 1 H, s, H-19), 6.02 and 6.38 (each 1 H, d, J = 11.0 Hz, H-7 and H-6, respectively). MS *m*/*z* 430 (M^+, 3), 412 (7), 394 (5), 371 (2),134 (87), 55 (100). UV (EtOH) λ_{max} 263 nm, λ_{min} 228 nm. HRMS calcd for $C_{28}H_{46}O_3$ 430.3447, found 430.3436.

22*S*-Butyl-1α,24-dihydroxy-24,25,26-trinorvitamin D_3 (4). The compound **4** was obtained from **14** (0.022 mmol) by the same procedure as described for **3** (yield 26%). The purity was proved to be more than 99% by two different HPLC systems: (1) YMC Pack ODS-AM 4.6 mm × 150 mm, H_2O/MeOH (15:85), 1.0 mL/min; (2) PEGASIL Silica SP100, 4.6 mm × 150 mm, hexane/$CHCl_3$/MeOH (100:25:10), 1.0 mL/min. ^1H NMR δ 0.55 (3 H, s,

H-18), 0.81 (3 H, d, $J = 6.7$ Hz, H-21), 0.90 (3 H, t, $J = 7.4$ Hz, CH_3 of Bu), 3.62 and 3.66 (each 1 H, m, H-24), 4.23 (1 H, m, H-3), 4.43 (1 H, m, H-1), 5.00 and 5.33 (each 1 H, m, H-19), 6.02 and 6.38 (each 1 H, d, $J = 11.0$ Hz, H-7 and H-6, respectively). MS *m/z* 430 (M^+, 4), 412 (7), 394 (5), 371 (2),134 (65), 55 (100). UV (EtOH) λ_{max} 264 nm, λ_{min} 228 nm. HRMS calcd for $C_{28}H_{46}O_3$ 430.3447, found 430.3438.

20*S*,22*R*-Butyl-(1α,3β)-chola-5,7-diene-1,3,24-triol (18). The compound **18** was obtained from **16** (0.08 mmol) by the same procedure as described for **13** (yield 62%). ^{1}H NMR δ 0.63 (3 H, s, H-18), 0.74 (3 H, d, $J = 6.1$ Hz, H-21), 0.90 (3 H, t, $J = 6.7$ Hz, CH_3 of Bu), 0.94 (3 H, s, H-19), 3.68 (2 H, m, H-24), 3.77 (1 H, m, H-1), 4.06 (1 H, m, H-3), 5.38 and 5.73 (each 1 H, m, H-6 and H-7). MS *m/z* 430 (M^+, 13), 412 (7), 394 (12), 371 (18), 55 (100). UV (EtOH) λ_{max} 272, 282, 294 nm.

20*S*,22*S*-Butyl-(1α,3β)-chola-5,7-diene-1,3,24-triol (17). The compound **17** was obtained from **15** (0.07 mmol) by the same procedure as described for **13** (yield 59%). ^{1}H NMR δ 0.60 (3 H, s, H-18), 0.74 (3 H, d, $J = 6.7$ Hz, H-21), 0.88 (3 H, t, $J = 7.3$ Hz, CH_3 of Bu), 0.91 (3 H, s, H-19), 3.56 and 3.72 (each 1 H, m, H-24), 3.77 (1 H, m, H-1), 4.22 (1 H, m, H-3), 5.24 and 5.59 (each 1 H, m, H-6 and H-7). MS *m/z* 430 (M^+, 13), 412 (7), 394 (13), 371 (20), 55 (100). UV (EtOH) λ_{max} 272, 282, 294 nm.

20*S*,22*R*-Butyl-1α,24-dihydroxy-24,25,26-trinorvitamin D_3 (6). The compound **6** was obtained from **18** (0.016 mmol) by the same procedure as described for **3** (yield 16%). The purity was proved to be more than 99% by two different HPLC systems: (1) YMC Pack ODS-AM 4.6 mm × 150 mm, H_2O/MeOH (15:85), 1.0 mL/min; (2) PEGASIL Silica SP100, 4.6 mm × 150 mm, hexane/$CHCl_3$/MeOH (100:25:10), 1.0 mL/min. ^{1}H NMR δ 0.53 (3 H, s, H-18), 0.74 (3 H, d, $J = 6.7$ Hz, H-21), 0.90 (3 H, t, $J = 6.7$ Hz, CH_3 of Bu), 3.62 and 3.67 (each 1 H, m, H-24), 4.23 (1 H, m, H-3), 4.43 (1 H, m, H-1), 5.00 and 5.33 (each 1 H, m, H-19), 6.02 and 6.38 (each 1 H, d, $J = 11.0$ Hz, H-7 and H-6, respectively). MS *m/z* 430 (M^+, 3), 412 (5), 394 (4), 134 (58), 55 (100). UV (EtOH) λ_{max} 264 nm, λ_{min} 229 nm. HRMS calcd for $C_{28}H_{46}O_3$ 430.3447, found 430.3473.

20*S*,22*S*-Butyl-1α,24-dihydroxy-24,25,26-trinorvitamin D_3 (5). The compound **5** was obtained from **17** (0.013 mmol) by the same procedure as described for **3** (yield 24%). The purity was proved to be more than 99% by two different HPLC systems: (1) YMC Pack ODS-AM 4.6 mm × 150 mm, H_2O/MeOH (15:85), 1.0 mL/min; (2) PEGASIL Silica SP100, 4.6 mm × 150 mm, hexane/$CHCl_3$/MeOH (100:25:10), 1.0 mL/min. ^{1}H NMR δ 0.54 (3 H, s, H-18), 0.72 (3 H, d, $J = 6.7$ Hz, H-21), 0.89 (3 H, t, $J = 6.7$ Hz, CH_3 of Bu), 3.63 and 3.72 (each 1 H, m, H-24), 4.23 (1 H, m, H-3), 4.43 (1 H, m, H-1), 5.00 and 5.33 (each 1 H, m, H-19), 6.02 and 6.38 (each 1 H, d, $J = 11.0$ Hz, H-7 and H-6, respectively). MS *m/z* 430 (M^+, 4), 412 (7), 394 (4), 134 (58), 55 (100). UV (EtOH) λ_{max} 264 nm, λ_{min} 228 nm. HRMS calcd for $C_{28}H_{46}O_3$ 430.3447, found 430.3434.

1α,3β-Bis[(methoxycarbonyl)oxy]-22*R*-butyl-5,7-choladiene-24-ol (19). To a solution of **11** (200 mg, 0.35 mmol) in THF (3 mL) was added diisobutyl-aluminum hydride (DIBAL, 1.0 M solution in toluene, 700 μL, 0.7 mmol) at −30 °C and the mixture was stirred for 1 h. Then, the mixture was allowed to 0 °C and was stirred for 3 h. The reaction mixture was poured into ice−water, extracted with ethyl acetate, washed with water, dried over Na_2SO_4, and evaporated. The residue was chromatographed on silica gel (C-200, 12 g) with 0.5% EtOH−CH_2Cl_2 to give **19** (122 mg, 64%). ^{1}H NMR δ 0.63 (3 H, s, H-18), 0.80 (3 H, d, $J = 6.9$ Hz, H-21), 0.90 (3 H, t, $J = 6.9$ Hz, CH_3 of *n*-Bu), 1.01 (3 H, s, H-19), 3.60 and 3.72 (each 1 H, m, H-24), 3.78 and 3.79 (each 3 H, s, CH_3OCO−), 4.84 (1 H, m, H-1), 4.91 (1 H, m, H-3), 5.38 and 5.69 (each 1 H, m, H-6 and H-7).

1α,3β-Bis[(methoxycarbonyl)oxy]-22*S*-butyl-5,7-choladiene-24-ol (20). The compound **20** was obtained from **12** (0.26 mmol) by the same procedure as described for **19** (yield 62%). ^{1}H NMR δ 0.61 (3 H, s, H-18), 0.82 (3 H, d, $J = 5.4$ Hz, H-21), 0.89 (3 H, t, $J = 6.9$ Hz, CH_3 of *n*-Bu), 1.01 (3 H, s, H-19), 3.66 (2 H, m, H-24), 3.78 and 3.79 (each 3 H, s, CH_3OCO−), 4.84 (1 H, m, H-1), 4.92 (1 H, m, H-3), 5.38 and 5.69 (each 1 H, m, H-6 and H-7). ^{13}C NMR δ 12.1, 13.5, 14.4, 16.3, 20.6, 23.1, 23.4, 28.3, 28.6, 31.0, 32.1, 35.5, 35.8, 36.6, 38.0, 38.2, 39.2, 41.4, 43.0, 53.3, 54.7, 54.9, 55.0, 62.0, 72.4, 78.6, 115.6, 122.4, 133.9, 141.4, 155.2, 155.3. MS *m/z* (%): 546 (M^+, 1), 470 (10), 394 (100), 251 (18), 224 (25), 209 (44), 197 (35), 167 (14), 157 (29), 149 (90), 141 (40), 129 (30), 115 (11), 105 (12). HRMS calcd for $C_{30}H_{46}O_4$ (M^+−$CH_3O(CO)OH$) 470.3396, found 470.3385. IR (neat) 3335, 2955, 2937, 2872, 1747, 1443, 1283, 1271, 1254, 1148 cm^{-1}.

1α,3β-Bis[(methoxycarbonyl)oxy]-22*R*-butyl-5,7-choladiene-24-al (21). To a solution of oxalyl chloride (15.5 μL, 0.18 mmol) in CH_2Cl_2 (0.8 mL) was added a solution of DMSO (27.4 μL, 0.39 mmol) in CH_2Cl_2 (0.2 mL) at −78 °C and the mixture was stirred at that temperature for 15 min. To this solution was added a solution of **19** (88 mg, 0.16 mmol) in CH_2Cl_2 (1.0 mL), and the mixture was stirred for 15 min. Triethylamine (112 μL, 0.81 mmol) was added to the reaction mixture at −78 °C, and then the mixture was allowed to warm to room temperature. The reaction mixture was diluted with CH_2Cl_2, washed with water, dried, and evaporated. The residue was chromatographed on silica gel (8 g) with 2.4% AcOEt−benzene to yield **21** (63 mg, 72%). ^{1}H NMR δ 0.64 (3 H, s, H-18), 0.82 (3 H, d, $J = 6.9$ Hz, H-21), 0.89 (3 H, t, $J = 6.9$ Hz, CH_3 of *n*-Bu), 1.01 (3 H, s, H-19), 3.78 and 3.79 (each 3 H, s, CH_3OCO−), 4.84 (1 H, m, H-1), 4.92 (1 H, m, H-3), 5.38 and 5.70 (each 1 H, m, H-6 and H-7), 9.76 (1 H, m, H-24).

1α,3β-Bis[(methoxycarbonyl)oxy]-22*S*-butyl-5,7-choladiene-24-al (22). The compound **22** was obtained from **20** (0.09 mmol) by the same procedure as described for **21** (yield 72%). ^{1}H NMR δ 0.59 (3 H, s, H-18), 0.82 (3 H, d, $J = 5.9$ Hz, H-21), 0.90 (3 H, t, $J = 6.9$ Hz, CH_3 of *n*-Bu), 1.01 (3 H, s, H-19), 3.78 and 3.79 (each 3 H, s, CH_3OCO−), 4.84 (1 H, m, H-1), 4.92 (1 H, m, H-3), 5.38 and 5.69 (each 1 H, m, H-6 and H-7), 9.74 (1 H, dd, $J = 2.5$, 1.5 Hz, H-24). ^{13}C NMR δ 12.0, 13.4, 14.3, 16.2, 20.6, 23.1, 23.2, 27.8, 28.0, 30.6, 32.0, 35.1, 35.7, 37.9, 39.2, 39.6, 41.4, 43.0, 47.5, 53.3, 54.7, 54.8, 55.0, 72.4, 78.6, 115.7, 122.3, 134.0, 141.1, 155.17, 155.23, 203.7. MS *m/z* (%): 544 (M^+, 1), 468 (10), 392 (100), 224 (24), 209 (40), 195 (13), 167 (23), 157 (22), 155 (29), 149 (45), 143 (10), 129 (12), 105 (10). HRMS calcd for $C_{30}H_{44}O_4$ (M^+−$CH_3O(CO)OH$) 468.3240, found 468.3230. IR (neat) 2955, 2858, 1744, 1441, 1271, 1252 cm^{-1}.

(1α,3β,22*R*,24*R*)-Bis[(methoxycarbonyl)oxy]-22-butylcholesta-5,7-dien-24-ol (23) and (1α,3β,22*R*,24*S*)-Bis[(methoxycarbonyl)oxy]-22-butylcholesta-5,7-dien-24-ol (24). To a solution of **21** (64 mg, 0.12 mmol) in THF (1 mL) was added isopropylmagnesium chloride (2.0 M solution in THF, 118 μL, 0.24 mmol) at room temperature and the mixture was stirred for 25 min. Then, the reaction was quenched with water. The mixture was extracted with ethyl acetate, washed with water, dried over Na_2SO_4, and evaporated. The residue was chromatographed on silica gel (C-200, 6 g) with 2−6% AcOEt−benzene to give **23** (25 mg, 36%) and **24** (29 mg, 42%) in this order. **23**: ^{1}H NMR δ 0.64 (3 H, s, H-18), 0.78 (3 H, d, $J = 6.7$ Hz, H-21), 0.90 (3 H, t, $J = 6.8$ Hz, CH_3 of *n*-Bu), 0.91 and 0.92 (each 3 H, d, $J = 6.7$ Hz, H-26 and -27), 1.02 (3 H, s, H-19), 3.35 (1 H, m, H-24), 3.77 and 3.79 (each 3 H, s, CH_3OCO−), 4.84 (1 H, m, H-1), 4.92 (1 H, m, H-3), 5.38 and 5.69 (each 1 H, m, H-6 and H-7). **24**: ^{1}H NMR δ 0.63 (3 H, s, H-18), 0.81 (3 H, d, $J = 6.7$ Hz, H-21), 0.90 (3 H, t, $J = 6.7$ Hz, CH_3 of *n*-Bu), 0.88 and 0.96 (each 3 H, d, $J = 6.7$ Hz, H-26 and -27), 1.02 (3 H, s, H-19), 3.48 (1 H, m, H-24), 3.77 and 3.79 (each 3 H, s, CH_3OCO−), 4.84 (1 H, m, H-1), 4.90 (1 H, m, H-3), 5.38 and 5.68 (each 1 H, m, H-6 and H-7).

(1α,3β,22*S*,24*R*)-Bis[(methoxycarbonyl)oxy]-22-butylcholesta-5,7-dien-24-ol (25) and (1α,3β,22*S*,24*S*)-Bis[(methoxycarbonyl)oxy]-22-butylcholesta-5,7-dien-24-ol (26). The compounds **25** (yield 34%) and **26** (yield 51%) were obtained from **22** (0.061 mmol) by the same procedure as described for **23** and **24**. **25**: ^{1}H NMR δ 0.63 (3 H, s, H-18), 0.78 (3 H, d, $J = 5.9$ Hz, H-21), 0.89 (3 H, t, $J = 6.9$ Hz, CH_3 of *n*-Bu), 0.93 (6H, d, $J = 6.4$ Hz, H-26 and -27), 1.02 (3 H, s, H-19), 3.39 (1 H, m, H-24), 3.78 and 3.79 (each 3 H, s, CH_3OCO−), 4.84 (1 H, m, H-1), 4.92 (1 H, m, H-3), 5.38 and 5.69 (each 1 H, m, H-6 and H-7). ^{13}C NMR δ 12.1, 13.2,

14.4, 16.3, 17.7, 19.0, 20.6, 23.2, 23.5, 28.4, 28.7, 30.8, 32.1, 34.6, 35.8, 36.00, 36.02, 36.9, 38.0, 39.2, 41.4, 43.1, 53.3, 54.8, 54.9, 55.1, 72.4, 74.1, 78.7, 115.7, 122.4, 133.9, 141.4, 155.2, 155.3. MS *m/z* (%): 588 (M^+, 1), 512 (5), 436 (85), 279 (15), 251 (12), 224 (23), 209 (37), 197 (27), 157 (19), 155 (28), 149 (100), 141 (26). HRMS calcd for $C_{33}H_{52}O_4$ ($M^+-CH_3O(CO)OH$) 512.3866, found 512.3861. IR (neat) 3572, 2955, 2872, 1745, 1443, 1344, 1283, 1254, 1148 cm^{-1}. **26**: ^1H NMR δ 0.61 (3 H, s, H-18), 0.83 (3 H, d, J = 6.4 Hz, H-21), 0.90 (3 H, t, J = 6.9 Hz, CH_3 of *n*-Bu), 0.89 and 0.95 (each 3 H, d, J = 6.9 Hz, H-26 and -27), 1.01 (3 H, s, H-19), 3.45 (1 H, m, H-24), 3.78 and 3.79 (each 3 H, s, CH_3OCO-), 4.84 (1 H, m, H-1), 4.92 (1 H, m, H-3), 5.38 and 5.69 (each 1 H, m, H-6 and H-7). ^{13}C NMR δ 12.1, 13.7, 14.4, 16.2, 16.3, 19.5, 20.6, 23.2, 23.5, 28.2, 29.1, 31.3, 32.1, 33.2, 35.8, 37.5, 38.0, 38.3, 39.2, 39.7, 41.4, 43.0, 53.6, 54.7, 54.8, 55.0, 72.4, 76.1, 78.7, 115.6, 122.4, 133.9, 141.4, 155.2, 155.3. MS *m/z* (%): 588 (M^+, 1), 512 (10), 436 (100), 251 (14), 249 (12), 223 (13), 210 (16), 197 (34), 183 (13), 157 (24), 155 (35), 143 (11), 141 (32), 129 (14). HRMS calcd for $C_{33}H_{52}O_4$ ($M^+-CH_3O(CO)OH$) 512.3866, found 512.3862. IR (neat) 3695, 2957, 2872, 1745, 1443, 1281, 1271, 1252 cm^{-1}.

(1α,3β,22*R*,24*R*)-22-butylcholesta-5,7-diene-1,3,24-triol (27). To a solution of **23** (28 mg, 0.048 mmol) in CH_2Cl_2 (0.6 mL) was added 5% KOH/MeOH (3.4 mL) and the mixture was stirred at 40 °C for 1.5 h. The reaction mixture was diluted with $CHCl_3$, washed with water, dried over Na_2SO_4, and evaporated. The residue was chromatographed on silica gel with 65% AcOEt−CH_2Cl_2 to give **27** (18 mg, 80%). ^1H NMR δ 0.65 (3 H, s, H-18), 0.80 (3 H, d, J = 6.7 Hz, H-21), 0.91 (3 H, t, J = 6.7 Hz, CH_3 of *n*-Bu), 0.91 and 0.93 (each 3 H, d, J = 6.7 Hz, H-26 and -27), 0.95 (3 H, s, H-19), 3.34 (1 H, m, H-24), 3.77 (1 H, m, H-1), 4.10 (1 H, m, H-3), 5.38 and 5.73 (each 1 H, m, H-6 and H-7). MS *m/z* 472 (M^+, 13), 454 (9), 436 (13), 413 (14), 55 (100). UV (EtOH) λ_{max} 272, 282, 294 nm.

Compounds 28−30. By the same procedure as described for **27**, each triol **28** (yield 57%), **29** (yield 60%), and **30** (yield 57%) was obtained from the corresponding precursors, **24** (0.043 mmol), **25** (0.026 mmol), and **26** (0.036 mmol), respectively.

(1α,3β,22*R*,24*S*)-22-butylcholesta-5,7-diene-1,3,24-triol (28). ^1H NMR δ 0.65 (3 H, s, H-18), 0.82 (3 H, d, J = 6.7 Hz, H-21), 0.90 (3 H, t, J = 7.3 Hz, CH_3 of *n*-Bu), 0.88 and 0.96 (each 3 H, d, J = 6.7 Hz, H-26 and -27), 0.95 (3 H, s, H-19), 3.49 (1 H, m, H-24), 3.77 (1 H, m, H-1), 4.09 (1 H, m, H-3), 5.38 and 5.73 (each 1 H, m, H-6 and H-7). MS *m/z* 472 (M^+, 14), 454 (10), 436 (15), 413 (19), 55 (100). UV (EtOH) λ_{max} 272, 282, 294 nm.

(1α,3β,22*S*,24*R*)-22-butylcholesta-5,7-diene-1,3,24-triol (29). ^1H NMR δ 0.64 (3 H, s, H-18), 0.80 (3 H, d, J = 5.9 Hz, H-21), 0.90 (3 H, t, J = 6.7 Hz, CH_3 of *n*-Bu), 0.93 (6 H, d, J = 6.7 Hz, H-26 and -27), 0.96 (3 H, s, H-19), 3.40 (1 H, m, H-24), 3.78 (1 H, m, H-1), 4.08 (1 H, m, H-3), 5.39 and 5.74 (each 1 H, m, H-6 and H-7). MS *m/z* 472 (M^+, 27), 454 (16), 436 (21), 413 (21), 55 (100). UV (EtOH) λ_{max} 272, 282, 294 nm.

(1α,3β,22*S*,24*S*)-22-butylcholesta-5,7-diene-1,3,24-triol (30). ^1H NMR δ 0.63 (3 H, s, H-18), 0.85 (3 H, d, J = 6.7 Hz, H-21), 0.90 (3 H, t, J = 6.7 Hz, CH_3 of *n*-Bu), 0.89 and 0.95 (each 3 H, d, J = 6.7 Hz, H-26 and -27), 0.95 (3 H, s, H-19), 3.46 (1 H, m, H-24), 3.77 (1 H, m, H-1), 4.07 (1 H, m, H-3), 5.39 and 5.73 (each 1 H, m, H-6 and H-7). MS *m/z* 472 (M^+, 15), 454 (11), 436 (17), 413 (19), 55 (100). UV (EtOH) λ_{max} 272, 282, 294 nm.

Compounds 7−10. By the same procedure as described for **3**, compounds **7** (yield 21%), **8** (yield 26%), **9** (yield 28%), and **10** (yield 27%) were obtained from the corresponding precursors, **27** (0.01 mmol), **28** (0.016 mmol), **29** (0.017 mmol), and **30** (0.011 mmol), respectively. The purity of compounds **7−10** was proved to be more than 99% by two different HPLC systems: (1) YMC Pack ODS-AM 4.6 mm × 150 mm, H_2O/MeOH (10:90), 1.0 mL/min; (2) PEGASIL Silica SP100, 4.6 mm × 150 mm, hexane/$CHCl_3$/MeOH (100:25:8), 1.0 mL/min.

(1α,22*R*,24*R*)-22-Butyl-1,24-dihydroxyvitamin D_3 (7). ^1H NMR δ 0.58 (3 H, s, H-18), 0.77 (3 H, d, J = 6.7 Hz, H-21), 0.90 (3 H, t, J = 6.7 Hz, CH_3 of *n*-Bu), 0.91 and 0.93 (each 3 H, d, J = 6.7 Hz, H-26 and -27), 3.35 (1 H, m, H-24), 4.23 (1 H, m, H-3), 4.43 (1 H, m, H-1), 5.01 and 5.33 (each 1 H, m, H-19), 6.02 and 6.38 (each 1 H, d, J = 11.0 Hz, H-7 and H-6, respectively). MS *m/z* 472 (M^+, 3), 454 (9), 436 (6), 152 (22),134 (72), 55 (100). UV (EtOH) λ_{max} 264 nm, λ_{min} 229 nm. HRMS calcd for $C_{31}H_{52}O_3$ 472.3916, found 472.3904.

(1α,22*R*,24*S*)-22-Butyl-1,24-dihydroxyvitamin D_3 (8). ^1H NMR δ 0.57 (3 H, s, H-18), 0.80 (3 H, d, J = 6.8 Hz, H-21), 0.89 (3 H, t, J = 6.7 Hz, CH_3 of *n*-Bu), 0.89 and 0.97 (each 3 H, d, J = 6.7 Hz, H-26 and -27), 3.49 (1 H, m, H-24), 4.23 (1 H, m, H-3), 4.43 (1 H, m, H-1), 5.00 and 5.33 (each 1 H, m, H-19), 6.02 and 6.38 (each 1 H, d, J = 11.0 Hz, H-7 and H-6, respectively). MS *m/z* 472 (M^+, 3), 454 (11), 436 (11), 152 (21),134 (77), 55 (100). UV (EtOH) λ_{max} 264 nm, λ_{min} 229 nm. HRMS calcd for $C_{31}H_{52}O_3$ 472.3916, found 472.3942.

(1α,22*S*,24*R*)-22-Butyl-1,24-dihydroxyvitamin D_3 (9). ^1H NMR δ 0.57 (3 H, s, H-18), 0.78 (3 H, d, J = 5.5 Hz, H-21), 0.90 (3 H, t, J = 6.7 Hz, CH_3 of *n*-Bu), 0.92 (6 H, d, J = 6.7 Hz, H-26 and −27), 3.38 (1 H, m, H-24), 4.23 (1 H, m, H-3), 4.43 (1 H, m, H-1), 5.00 and 5.33 (each 1 H, s, m, H-19), 6.02 and 6.38 (each 1 H, d, J = 11.0 Hz, H-7, H-6, respectively. MS *m/z* 472 (M^+, 4), 454 (9), 436 (6), 152 (23),134 (76), 55 (100). UV (EtOH) λ_{max} 265 nm, λ_{min} 228 nm. HRMS calcd for $C_{31}H_{52}O_3$ 472.3916, found 472.3893.

(1α,22*S*,24*S*)-22-Butyl-1,24-dihydroxyvitamin D_3 (10). ^1H NMR δ 0.55 (3 H, s, H-18), 0.83 (3 H, d, J = 5.4 Hz, H-21), 0.90 (3 H, t, J = 7.4 Hz, CH_3 of *n*-Bu), 0.89 and 0.95 (each 3 H, d, J = 6.7 Hz, H-26 and -27), 3.45 (1 H, m, H-24), 4.23 (1 H, m, H-3), 4.43 (1 H, m, H-1), 5.01 and 5.33 (each 1 H, m, H-19), 6.02 and 6.38 (each 1 H, d, J = 11.0 Hz, H-7 and H-6, respectively). MS *m/z* 472 (M^+, 3), 454 (9), 436 (5), 152 (22),134 (76), 55 (100). UV (EtOH) λ_{max} 265 nm, λ_{min} 229 nm. HRMS calcd for $C_{31}H_{52}O_3$ 472.3916, found 472.3893.

(3*R*,5*R*)-5-(1-{(1*S*,3*R*,10*R*,13*R*,17*R*)-1,3-bis[(methoxycarbonyl)oxy]-10,13-dimethyl-2,3,4,9,10,11,12,13,14,15,16,17-dodecahydro-1*H*-cyclopenta[a]phenanthren-17-yl}ethyl)-2-methylnonan-3-yl (2*S*)-3,3,3-Trifluoro-2-methoxy-2-phenylpropanoate (31). To a solution of compound **23** (6.1 mg, 0.010 mmol) in dry CH_2Cl_2 (100 μL) were added Et_3N (30 μL, 0.21 mmol), a solution of *R*-MTPACl (20 μL, 0.10 mmol) in dry CH_2Cl_2 (60 μL), and DMAP (15.5 mg, 0.13 mmol), and the reaction mixture was stirred for 30 min at room temperature. The reaction was quenched with H_2O at 0 °C and was extracted with AcOEt. The organic layer was washed with brine, dried over $MgSO_4$, and evaporated. The residue was chromatographed on silica gel (5 g, hexane/AcOEt = 4/1) to give *S*-MTPA ester **31** (5.8 mg, 69.6%). **31**: ^1H NMR δ 0.57 (3 H, s, H-18), 0.76 (3 H, d, J = 6.7 Hz, H-21), 0.84 and 0.89 (each 3 H, d, J = 6.9 Hz, H-26, 27), 0.90 (3 H, t, J = 7.2 Hz, CH_3 of Bu), 1.01 (3 H, s, H-19), 3.49 (3 H, s, OCH_3), 3.776 and 3.784 (each 3 H, s, $O(CO)OCH_3$), 4.84 (1 H, m, H-1), 4.90 (1 H, m, H-3), 5.08 (1 H, dd, J = 10.3, 1.7 Hz, H-24), 5.36 (1 H, dd, J = 5.6, 2.9 Hz, H-7), 5.69 (1 H, dd, J = 5.6, 1.9 Hz, H-6), 7.40 (3 H, m, Ph-3, 4, 5), 7.53 (2 H, m, Ph-2, 6).

(3*R*,5*R*)-5-(1-{(1*S*,3*R*,10*R*,13*R*,17*R*)-1,3-bis[(methoxycarbonyl)oxy]-10,13-dimethyl-2,3,4,9,10,11,12,13,14,15,16,17-dodecahydro-1*H*-cyclopenta[a]phenanthren-17-yl}ethyl)-2-methylnonan-3-yl (2*R*)-3,3,3-Trifluoro-2-methoxy-2-phenylpropanoate (32). In a similar manner to that for the synthesis of **31** from **23**, a crude product was obtained from **23** (14.4 mg, 0.024 mmol), Et_3N (36 μL, 0.24 mmol), *S*-MTPACl (23 μL, 0.24 mmol), and DMAP (18.7 mg, 0.15 mmol) in dry CH_2Cl_2 at room temperature for 30 min and was purified by chromatographed on silica gel (5 g, hexane/AcOEt = 4/1) to give *R*-MTPA ester **32** (5.8 mg, 29.5%). **32**: ^1H NMR δ 0.53 (3 H, s, H-18), 0.72 (3 H, d, J = 6.7 Hz, H-21), 0.92 (3 H, t, J = 7.1 Hz, CH_3 of Bu), 0.93 (6 H, d, J = 6.9 Hz, H-26, 27), 1.00 (3 H, s, H-19), 3.58 (3 H, s, OCH_3), 3.776 and 3.779 (each 3 H, s, $O(CO)OCH_3$), 4.83 (1 H, m, H-1), 4.89 (1 H, m, H-3), 5.09 (1 H, dd, J = 9.6, 3.7 Hz, H-24), 5.35 (1 H, dd, J = 5.6, 2.9 Hz, H-7), 5.69 (1 H, dd, J = 5.6, 1.8 Hz, H-6), 7.39 (3 H, m, Ph-3, 4, 5), 7.55 (2 H, m, Ph-2, 6).

(3*S*,5*S*)-5-(1-{(1*S*,3*R*,10*R*,13*R*,17*R*)-1,3-bis[(methoxycarbonyl)oxy]-10,13-dimethyl-2,3,4,9,10,11,12,13,14,15,16,17-dodecahydro-1*H*-cyclopenta[a]phenanthren-17-yl}ethyl)-2-methylnonan-3-yl (2*S*)-3,3,3-Trifluoro-2-methoxy-2-phenylpropanoate (33). Compound **33** was obtained from **26** (0.01 mmol) by the same procedure as described for **31** (yield 97.1%). **33**: ^{1}H NMR δ 0.59 (3 H, s, H-18), 0.83 (3 H, d, J = 6.1 Hz, H-21), 0.90 (3 H, t, J = 6.8 Hz, CH_3 of Bu), 0.91 and 0.93 (each 3 H, d, J = 6.9 Hz, H-26, 27), 1.01 (3 H, s, H-19), 3.53 (3 H, s, OCH_3), 3.78 and 3.79 (each 3 H, s, O(CO)OCH_3), 4.85 (1 H, m, H-1), 4.90 (1 H, m, H-3), 5.04 (1 H, m, H-24), 5.37 (1 H, m, H-7), 5.69 (1 H, dd, J = 5.6, 2.0 Hz, H-6), 7.39 (3 H, m, Ph-3, 4, 5), 7.54 (2 H, m, Ph-2, 6).

(3*S*,5*S*)-5-(1-{(1*S*,3*R*,10*R*,13*R*,17*R*)-1,3-bis[(methoxycarbonyl)oxy]-10,13-dimethyl-2,3,4,9,10,11,12,13,14,15,16,17-dodecahydro-1*H*-cyclopenta[*a*]phenanthren-17-yl}ethyl)-2-methylnonan-3-yl (2*R*)-3,3,3-trifluoro-2-methoxy-2-phenylpropanoate (34). Compound **34** was obtained from **26** (0.01 mmol) by the same procedure as described for **32** (yield 93.1%). **34**: ^{1}H NMR δ 0.61 (3 H, s, H-18), 0.83 (3 H, d, J = 6.8 Hz, H-21), 0.85 and 0.88 (each 3 H, d, J = 6.7 Hz, H-26, 27), 0.90 (3 H, t, J = 6.8 Hz, CH_3 of Bu), 1.01 (3 H, s, H-19), 3.56 (3 H, s, OCH_3), 3.78 and 3.79 (each 3 H, s, O(CO)OCH_3), 4.84 (1 H, m, H-1), 4.91 (1 H, m, H-3), 5.05 (1 H, m, H-24), 5.37 (1 H, m, H-7), 5.69 (1 H, dd, J = 5.6, 1.9 Hz, H-6), 7.40 (3 H, m, Ph-3, 4, 5), 7.56 (2 H, m, Ph-2, 6).

Competitive Binding Assay, Bovine Thymus VDR. Binding to bovine thymus VDR was evaluated according to the procedure reported.[20] Bovine thymus VDR was purchased from Yamasa Biochemical (Choshi, Chiba, Japan) and dissolved in 0.05 M phosphate buffer (pH 7.4) containing 0.3 M KCl and 5 mM dithiothreitol just before use. The receptor solution (500 μL) in an assay tube was incubated with 0.072 nM [^{3}H]-1,25-$(OH)_2D_3$ together with graded amounts of each vitamin D analogue (0.001−20 nM) or vehicle for 19 h at 4 °C. The bound and free [^{3}H]-1,25-$(OH)_2D_3$ were separated by treating with dextran-coated charcoal for 20 min at 4 °C. The assay tubes were centrifuged at 1000*g* for 10 min. The radioactivity of the supernatant was counted. Nonspecific binding was subtracted. These experiments were done in duplicate.

Transfection and Transactivation Assay. COS-7 cells were cultured in Dulbecco's modified Eagle's medium (DMEM) supplemented with 5% fetal bovine serum (FBS). Cells were seeded on 24-well plates at a density of 2 × 10^4 per well. After 24 h, the cells were transfected with a reporter plasmid containing three copies of the mouse osteopontin VDRE (5′-GGTTCAcgaGGTTCA, SPPx3-TK-Luc), a wild-type or mutant hVDR expression plasmid (pCMX-hVDR), and the internal control plasmid containing sea pansy luciferase expression constructs (pRL-CMV) by the lipofection method as described previously.[32] After 8 h of incubation, the cells were treated with either the ligand or ethanol vehicle and cultured for 16 h. Cells in each well were harvested with a cell lysis buffer, and the luciferase activity was measured with a luciferase assay kit (Promega, Wisconsin). Transactivation measured by the luciferase activity was normalized with the internal control. All experiments were done in triplicate.

Quantitative Real-Time RT-PCR Analysis. Total RNAs from samples were prepared with RNAgents Total RNA Isolation system (Promega), and cDNAs were synthesized using the ImProm-II reverse transcription system (Promega). Real-time PCR was performed on the ABI PRISM 7300 sequence detection system (Applied Biosystems, Foster City, CA) using SYBR Green Realtime PCR Master Mix -Plus- (Toyobo, Osaka, Japan). Primers were as follows: CYP24A1, 5′-TGA ACG TTG GCT TCA GGA GAA-3′ and 5′-AGG GTG CCT GAG TGT AGC ATC T-3′; actin, 5′-GAC AGG ATG CAG AAG GAG AT-3′ and 5′-GAA GCA TTT GCG GTG GAC GAT-3′. The RNA values were normalized to the level of Actin mRNA and represent the mean ± SD of triplicate assays.

Differentiation of HL-60 Cells. Human promyelocytic leukemia cells (HL-60) were plated at 2 × 10^5 cells/plate and were cultured in Eagle's modified medium as described previously.[33] The cells were incubated with each vitamin D compound (10^{-6}, 10^{-7} and 10^{-8} M) for 4 days. The differentiation activity was determined by an NBT reduction assay method as previously reported.[33,34] The experiments were done in duplicate.

X-ray Crystallographic Analysis of the Complex Structure. In this study, the method reported by Vanhooke et al.[6] was used with some modifications to prepare the crystals of VDR complexes. The rat VDR−LBD (residues 116−423, Δ165−211) was cloned as an N-terminal His_6-tagged fusion protein into the pET14b expression vector and overproduced in *Escherichia coli* C41. The cells were grown at 37 °C in LB medium (including ampicilin 100 mg/L) and subsequently induced for 6 h with 15 μM isopropyl-β-D-thiogalactopyranoside (IPTG) at 23 °C. The purification procedure included affinity chromatography on a Ni-NTA column, followed by dialysis and cation-exchange chromatography (SP-Sepharose). After tag removal by thrombin digestion, protease was removed by filtration through a HiTrap benzamidine column and the protein was further purified by gel filtration on a Superdex200 column. The purity and homogeneity of the rVDR−LBD were assessed by SDS-PAGE.

Purified rVDR−LBD solution was concentrated to about 0.75 mg/mL by ultrafiltration. To an aliquot (800 μL) of the protein solution was added a ligand (ca. 10 equiv), the solution was further concentrated to about 1/8, and then a solution (25 mM Tris-HCl, pH 8.0; 50 mM NaCl; 10 mM DTT; 0.02% NaN_3) of coactivator peptide (H_2N-KNHPMLMNLLKDN-$CONH_2$) derived from DRIP205 was added. This solution of VDR/ligand/peptide was allowed to crystallize by the vapor diffusion method using a series of precipitant solutions containing 0.1 M MOPS−NaOH (pH7.0), 0.1−0.4 M sodium formate, 12−22% (w/v) PEG4000, and 5% (v/v) ethylene glycol. Droplets for crystallization were prepared by mixing 2 μL of complex solution and 1 μL precipitant solution, and droplets were equilibrated against 500 μL precipitant solution at 20 °C. It took 1−2 days to obtain reproducible crystals with X-ray diffraction quality for VDR complex with the ligand **5**. On the other hand, the VDR complex with the ligand **4** gave only crystals of poor quality except the one used for the structure determination, which was barely suitable for X-ray diffraction experiment.

Prior to diffraction data collection, crystals were soaked in a cryoprotectant solution containing 0.1 M MOPS−NaOH (pH 7.0), 0.1−0.4 M sodium formate, 15−20% PEG4000, and 17−20% ethylene glycol. Diffraction data sets were collected at 100 K in a stream of nitrogen gas at beamline BL-6A of KEK-PF (Tsukuba, Japan). Reflections were recorded with an oscillation range per image of 1.0°. Diffraction data were indexed, integrated, and scaled using the program HKL2000.[35] The structures of complex were solved by molecular replacement with the program CNS[36] using a rat VDR−LBD coordinates (PDB code: 1RK3), and finalized sets of atomic coordinates were obtained after iterative rounds of model modification with the program XtalView[37] and refinement with CNS by rigid body refinement, simulated annealing, positional minimization, water molecule identification, and individual isotropic B-value refinement. The coordinates of the two complexes were deposited in the Protein Data Bank with accession number 2ZXM for ligand **4** and 2ZXN for ligand **5**.

Graphical Manipulations and Ligand Docking. Graphical manipulations were performed using SYBYL 8.0 (Tripos, St. Louis). The atomic coordinates of the crystal structure of zVDR-LBD complexed with GEMINI (**1b**) were retrieved from Protein Data Bank (PDB) (entry 2HCD).[11] 22-Butyl vitamin D analogues (**3**, **6**, **7**−**10**) were docked into the ligand-binding pocket using Surflex Dock 2.0 (Tripos, St. Louis), and then the docking models were modified to agree with the biological activities.

Acknowledgment. Part of this work was supported by a Grant-in-Aid for Scientific Research (no. 20590108) from the Ministry of Education, Culture, Sports, Science, and Technology, Japan.

Supporting Information Available: Transcriptional activities in HEK293 cells, ASMA, recruitment of RXR and SRC-1, and

HPLC charts to prove purity of compounds **3**–**10**. This material is available free of charge via the Internet at http://pubs.acs.org.

References

(1) Feldman, D.; Pike, J. W. Glorieux, F. H. , Eds. *Vitamin D*, 2nd ed.; Elsevier Academic Press: New York, 2005.

(2) Jurutka, P. W.; Whitfield, G. K.; Hsieh, J. C.; Thompson, P. D.; Haussler, C. A.; Haussler, M. R. Synthesis and Conformational Analysis of 17α,21-Cyclo-22-Unsaturated Analogues of Calcitriol. *Rev. Endocr. Metab. Disord.* **2001**, *2*, 203–216.

(3) Yamada, S.; Shimizu, M.; Yamamoto, K. Vitamin D Receptor. In *Vitamin D and Rickets, Endocrine Development*, Vol. 6; Hochberg, Z., Ed.; Karger: Basel, Switzerland, 2003; pp 50–68.

(4) Rochel, N.; Wurtz, J. M.; Mitschler, A.; Klaholz, B.; Moras, D. The Crystal Structure of the Nuclear Receptor for Vitamin D Bound to Its Natural Ligand. *Mol. Cell* **2000**, *5*, 173–179.

(5) Tocchini-Valentini, G.; Rochel, N.; Wurtz, J. M.; Mitschler, A.; Moras, D. Crystal structures of the vitamin D receptor complexed to super agonist 20-epi ligands. *Proc. Natl. Acad. Sci. U.S.A.* **2001**, *98*, 5491–5496.

(6) Vanhooke, J. L.; Benning, M. M.; Bauer, C. B.; Pike, J. W.; DeLuca, H. F. Molecular Structure of the Rat Vitamin D Receptor Ligand Binding Domain Complexed with 2-Carbon-Substituted Vitamin D_3 Hormone Analogues and a LXXLL-Containing Coactivator Peptide. *Biochemistry* **2004**, *43*, 4101–4110.

(7) Ciesielski, F.; Rochel, N.; Mitschler, A.; Kouzmenko, A.; Moras, D. Structural investigation of the ligand binding domain of the zebrafish VDR in complexes with 1 α,25$(OH)_2D_3$ and Gemini: purification, crystallization and preliminary X-ray diffraction analysis. *J. Steroid Biochem. Mol. Biol.* **2004**, *89–90*, 55–59.

(8) Tocchini-Valentini, G.; Rochel, N.; Wurtz, J.-M.; Moras, D. Crystal Structures of the Vitamin D Nuclear Receptor Liganded with the Vitamin D Side Chain Analogues Calcipotriol and Seocalcitol, Receptor Agonists of Clinical Importance. Insights into a Structural Basis for the Switching of Calcipotriol to a Receptor Antagonist by Further Side Chain Modification. *J. Med. Chem.* **2004**, *47*, 1956–1961.

(9) Eelen, G.; Verlinden, L.; Rochel, N.; Claessens, F.; De Clercq, P.; Vandewalle, M.; Tocchini-Valentini, G.; Moras, D.; Bouillon, R.; Verstuyf, A. Superagonistic action of 14-epi-analogs of 1,25-dihydroxyvitamin D explained by vitamin D receptor–coactivator interaction. *Mol. Pharmacol.* **2005**, *67*, 1566–73.

(10) Hourai, S.; Fujishima, T.; Kittaka, A.; Suhara, Y.; Takayama, H.; Rochel, N.; Moras, D. Probing a water channel near the A-ring of receptor-bound 1α,25-dihydroxyvitamin D_3 with selected 2α-substituted analogues. *J. Med. Chem.* **2006**, *49*, 5199–5205.

(11) Ciesielski, F.; Rochel, N.; Moras, D. Adaptability of the Vitamin D nuclear receptor to the synthetic ligand Gemini: remodelling the LBP with one side chain rotation. *J. Steroid Biochem. Mol. Biol.* **2007**, *103*, 235–42.

(12) Rochel, N.; Hourai, S.; Perez-Garcia, X.; Rumbo, A.; Mourino, A.; Moras, D. Crystal structure of the vitamin D nuclear receptor ligand binding domain in complex with a locked side chain analog of calcitriol. *Arch. Biochem. Biophys.* **2007**, *460*, 172–176.

(13) Vanhooke, J. L.; Tadi, B. P.; Benning, M. M.; Plum, L. A.; DeLuca, H. F. New analogs of 2-methylene-19-nor-(20*S*)-1,25-dihydroxyvitamin D_3 with conformationally restricted side chains: evaluation of biological activity and structural determination of VDR-bound conformations. *Arch. Biochem. Biophys.* **2007**, *460*, 161–165.

(14) Hourai, S.; Rodrigues, L. C.; Antony, P.; Reina-San-Martin, B.; Ciesielski, F.; Magnier, B. C.; Schoonjans, K.; Mourino, A.; Rochel, N.; Moras, D. Structure-based design of a superagonist ligand for the vitamin D nuclear receptor. *Chem. Biol.* **2008**, *15*, 383–392.

(15) Shimizu, M.; Miyamoto, Y.; Takaku, H.; Matsuo, M.; Nakabayashi, M.; Masuno, H.; Udagawa, N.; DeLuca, H. F.; Ikura, T.; Ito, N. 2-Substituted-16-ene-22-thia-1α,25-dihydroxy-26,27-dimethyl-19-norvitamin D_3 analogs: Synthesis, biological evaluation, and crystal structure. *Bioorg. Med. Chem.* **2008**, *16*, 6949–6964.

(16) Nakabayashi, M.; Yamada, S.; Yoshimoto, N.; Tanaka, T.; Igarashi, M.; Ikura, T.; Ito, N.; Makishima, M.; Tokiwa, H.; Deluca, H. F.; Shimizu, M. Crystal Structures of Rat Vitamin D Receptor Bound to Adamantyl Vitamin D Analogs: Structural Basis for Vitamin D Receptor Antagonism and Partial Agonism. *J. Med. Chem.* **2008**, *51*, 5320–5329.

(17) Uskokovic, M. R.; Manchand, P. S.; Peleg, S.; Norman, A. W. Synthesis and preliminary evaluation of the biological properties of a 1α,25-dihydroxyvitamin D3 analogue with two side chains. In *Vitamin D: Chemistry, Biology and Clinical Applications of the Steroid Hormone*; Norman, A. W., Bouillon, R., Thomasset, M., Eds.; University of California: Riverside, 1997; pp19–21.

(18) Kurek-Tyrlik, A.; Makaev, F. Z.; Wicha, J.; Zhabinskii, V.; Calverley, M. J. Pivoting 20-Normal and 20-Epi Calcitriols: Synthesis and Crystal Structure of a "Double Side Chain" Analogue. In *Vitamin D: Chemistry, Biology and Clinical Applications of the Steroid Hormone*; Norman, A. W., Bouillon, R., Thomasset, M., Eds.; University of California: Riverside, 1997; pp30–31.

(19) Norman, A. W.; Manchand, P. S.; Uskokovic, M. R.; Okamura, W. H.; Takeuchi, J. A.; Bishop, J. E.; Hisatake, J. I.; Koeffler, H. P.; Peleg, S. Characterization of a novel analogue of 1α,25$(OH)_2$-vitamin D_3 with two side chains: interaction with its nuclear receptor and cellular actions. *J. Med. Chem.* **2000**, *43*, 2719–2730.

(20) Yamamoto, K.; Sun, W.-Y.; Ohta, M.; Hamada, K.; DeLuca, H. F.; Yamada, S. Conformationally Restricted Analogs of 1α,25-Dihydroxyvitamin D_3 and Its 20-Epimer: Compounds for Study of the Three-Dimensional Structure of Vitamin D Responsible for Binding to the Receptor. *J. Med. Chem.* **1996**, *39*, 2727–2737.

(21) Yamamoto, K.; Ooizumi, H.; Umesono, K.; Verstuyf, A.; Bouillon, R.; DeLuca, H. F.; Shinki, T.; Suda, T.; Yamada, S. Three-dimensional structure-function relationship of vitamin D: side chain location and various activities. *Bioorg. Med. Chem. Lett.* **1999**, *9*, 1041–1046.

(22) Yamamoto, K.; Inaba, Y.; Yoshimoto, N.; Choi, M.; DeLuca, H. F.; Yamada, S. 22-Alkyl-20-epi-1α,25-dihydroxyvitamin D_3 Compounds of Super-agonistic Activity: Syntheses, Biological Activities and Interaction with the Receptor. *J. Med. Chem.* **2007**, *50*, 932–939.

(23) Yoshimoto, N.; Inaba, Y.; Yamada, S.; Makishima, M.; Shimizu, M.; Yamamoto, K. 2-Methylene 19-nor-25-dehydro-1α-hydroxyvitamin D_3 26,23-lactones: Synthesis, biological activities and molecular basis of passive antagonism. *Bioorg. Med. Chem.* **2008**, *16*, 457–473.

(24) Yamamoto, K.; Ogura, H.; Jukuta, J.; Inoue, H.; Hamada, K.; Sugiyama, Y.; Yamada, S. Stereochemical and Mechanistic Studies on Conjugate Addition of Organocuprates to Acyclic Enones and Enoates: Simple Rule for Diastereofacial Selectivity. *J. Org. Chem.* **1998**, *63*, 4449–4458.

(25) Ohtani, I.; Kusumi, T.; Kashman, Y.; Kakisawa, H. *J. Am. Chem. Soc.* **1991**, *113*, 4092.

(26) GenBank accession no. Q28037.

(27) GenBank accession no. P11473.

(28) Peleg, S.; Liu, Y. Y.; Reddy, S.; Horst, R. L.; White, M. C.; Posner, G. H. A 20-epi side chain restores growth-regulatory and transcriptional activities of an A ring-modified hybrid analog of 1α,25-dihydroxyvitamin D_3 without increasing its affinity to the vitamin D receptor. *J. Cell. Biochem.* **1996**, *63*, 149–161.

(29) (a) Haussler, M. R.; Whitfield, G. K.; Haussler, C. A.; Hsieh, J. C.; Thompson, P. D.; Selznick, S. H.; Dominguez, C. E.; Jurutka, P. W. The nuclear vitamin D receptor: biological and molecular regulatory properties revealed. *J. Bone Miner. Res.* **1998**, *13*, 325–349. (b) Abe, E.; Miyaura, C.; Sakagami, H. I.; Takeda, M; Konno, K.; Yamazaki, T.; Yoshiki, S.; Suda, T. Differentiation of mouse myeloid leukemia cells induced by 1α,25-dihydroxyvitamin D_3. *Proc. Natl. Acad. Sci. U.S.A.* **1981**, *78*, 4990–4994.

(30) Yamamoto, K.; Abe, D.; Yoshimoto, N.; Choi, M.; Yamagishi, K.; Tokiwa, H.; Shimizu, M.; Makishima, M.; Yamada, S. Vitamin D Receptor: Ligand Recognition and Allosteric Network. *J. Med. Chem.* **2006**, *49*, 1313–1324.

(31) Inaba, Y.; Yamamoto, K.; Yoshimoto, N.; Matsunawa, M.; Uno, S.; Yamada, S.; Makishima, M. Vitamin D_3 derivatives with adamantane or lactone ring side chains are cell type-selective vitamin D receptor modulators. *Mol. Pharmacol.* **2007**, *71*, 1298.

(32) Yamamoto, K.; Masuno, H.; Choi, M.; Nakashima, K.; Taga, T.; Ooizumi, H.; Umesono, K.; Sicinska, W.; Van Hooke, J.; DeLuca, H. F.; Yamada, S. Three-dimensional modeling of and ligand docking to vitamin D receptor ligand binding domain. *Proc. Natl. Acad. Sci. U.S.A.* **2000**, *97*, 1467–1472.

(33) Sicinski, R. R.; Prahl, J. M.; Smith, C. M.; DeLuca, H. F. New 1α,25-dihydroxy-19-norvitamin D_3 compounds of high biological activity: Synthesis and biological evaluation of 2-hydroxymethyl, 2-methyl, and 2-methylene analogues. *J. Med. Chem.* **1998**, *41*, 4662–4674.

(34) Sicinski, R. R.; Perlman, K. L.; Prahl, J.; Smith, C.; DeLuca, H. F. Synthesis and biological activity of 1α,25-dihydroxy-18-norvitamin D_3 and 1α,25-dihydroxy-18,19-dinorvitamin D_3. *J. Med. Chem.* **1996**, *39*, 4497–4506.

(35) Otwinowski, Z.; Minor, W. Processing of X-ray diffraction data collected in oscillation mode. *Methods Enzymol.* **1997**, *276*, 307–326.

(36) Brünger, A. T.; Adams, P. D.; Clore, G. M.; DeLano, W. L.; Gros, P.; Grosse-Kunstleve, R. W.; Jiang, J.-S.; Kuszewski, J.; Nilges, M.; Pannu, N. S.; Read, R. J.; Rice, L. M.; Simonson, T.; Warren, G. L. Crystallography & NMR system: a new software suite for macromolecular structure determination. *Acta Crystallogr., Sect. D: Biol. Crystallogr.* **1998**, *54*, 905–921.

(37) McRee, D. E. XtalView/Xfits a versatile program for manipulating atomic coordinates and electron density. *J. Struct. Biol.* **1999**, *125*, 156–165.

JM8014348

Structure-activity relationship study on artificial CXCR4 ligands possessing the cyclic pentapeptide scaffold: the exploration of amino acid residues of pentapeptides by substitutions of several aromatic amino acids†

Tomohiro Tanaka,[a] Wataru Nomura,*[a] Tetsuo Narumi,[a,b] Ai Esaka,[b] Shinya Oishi,[b] Nami Ohashi,[a] Kyoko Itotani,[a] Barry J. Evans,[c] Zi-xuan Wang,[c,d] Stephen C. Peiper,[c] Nobutaka Fujii[b] and Hirokazu Tamamura*[a]

Received 30th April 2009, Accepted 9th June 2009
First published as an Advance Article on the web 20th July 2009
DOI: 10.1039/b908286g

Previously, downsizing of a 14-residue peptidic CXCR4 antagonist **1** has led to the development of a highly potent CXCR4 antagonist **2** [*cyclo*(-D-Tyr[1]-Arg[2]-Arg[3]-Nal[4]-Gly[5]-)]. In the present study, cyclic pentapeptide libraries that were designed by substitutions of several amino acids for D-Tyr[1] and Arg[2] in peptide **2** were prepared and screened to evaluate binding activity for CXCR4. The above structure-activity relationship study led to the finding of several potent CXCR4 ligands.

Introduction

The chemokine receptor CXCR4, which has an endogenous ligand, stromal-cell derived factor-1α (SDF-1α)/CXCL12,[1,2] belongs to the G-protein coupled receptor (GPCR) family.[3,4] The CXCR4-CXCL12 axis plays an important role in various physiological functions: chemotaxis,[5] angiogenesis[6,7] and neurogenesis[8,9] in embryonic stage. However, CXCR4 is also relevant to multiple intractable diseases: AIDS,[10,11] cancer metastasis,[12] progress of leukemia,[13] and rheumatoid arthritis[14] in adulthood. Thus, CXCR4 is thought to be an attractive drug target against these diseases, and CXCR4 antagonists would be useful for the development of potent therapeutic agents.[15–17] Various CXCR4 antagonists such as AMD3100[18,19] and KRH-1636[20] have been reported to date. A 14-residue cyclic peptide CXCR4 antagonist **1** was previously found by structure optimization of an 18-residue bicyclic peptide polyphemusin analogue (Fig. 1).[21,22] Furthermore, the downsizing of **1** using its pharmacophore residues [Arg × 2, L-3-(2-naphthyl)alanine (Nal), Tyr] brought the development of cyclic pentapeptide **2** as a CXCR4 antagonist.[23]

In addition, a biologically stable analogue **3** was derived from **1** with the addition of a 4-fluorobenzoyl group as a new pharmacophore moiety at the N-terminus.[24] We have studied structure-activity-relationship (SAR) of **2** through various modifications such as changes of the ring size and amino acid substitutions.[25–27]

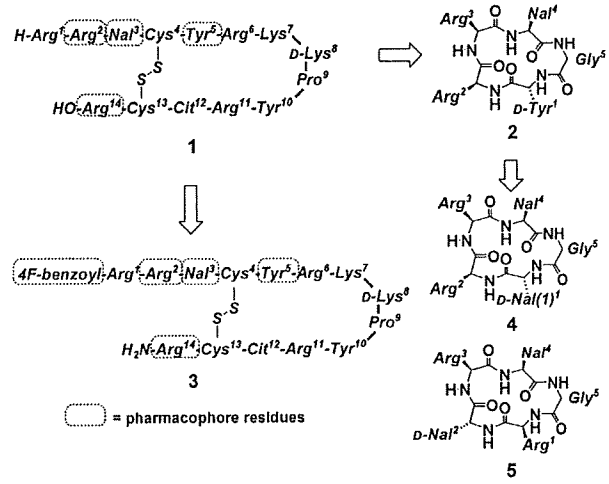

Fig. 1 Development of a cyclic pentapeptide **2** based on the pharmacophore of a CXCR4 antagonistic peptide **1**. Further conversion from **1** into a biostable derivative **3** and from **2** into new cyclic pentapeptide leads **4** and **5**. Cit = L-citrulline, Nal = L-3-(2-naphthyl)alanine, Nal(1) = L-3-(1-naphthyl)alanine.

Potent CXCR4 ligands contain aromatic and cationic groups,[28] suggesting that these groups are involved in binding to CXCR4 mediated by hydrophobic and electrostatic interactions. In a previous study, D-Tyr[1] and Arg[2] in peptide **2** were replaced by a bicyclic aromatic amino acid and a cationic amino acid to identify novel pharmacophores and to find new lead compounds. Compounds **4**, with replacement of D-Tyr[1] by D-3-(1-naphthyl)alanine (D-Nal(1)), and **5** with the sequence of Arg[1]-D-Nal[2] based on shuffling cationic and aromatic amino acids at positions 1 and 2 of compound **2** showed high CXCR4 binding activity.[29] Thus, in this study, the design of a cyclic pentapeptide library based on substitutions of several aromatic amino acids at positions 1 and 2 led to the development of novel analogues of **2** to explore new pharmacophore moieties.

[a]*Institute of Biomaterials and Bioengineering, Tokyo Medical and Dental University, Chiyoda-ku, Tokyo, 101-0062, Japan. E-mail: nomura.mr@tmd.ac.jp, tamamura.mr@tmd.ac.jp; Fax: +813 5280 8039; Tel: +813 5280 8036*
[b]*Graduate School of Pharmaceutical Sciences, Kyoto University, Sakyo-ku, Kyoto, 606-8501, Japan*
[c]*Department of Pathology, Anatomy and Cell Biology, Thomas Jefferson University, Philadelphia, PA 19107, USA*
[d]*Department of Surgery, Thomas Jefferson University, Philadelphia, PA 19107, USA*

† Electronic supplementary information (ESI) available: Characterization data (MS and $[\alpha]_D$) and HPLC charts of novel synthetic compounds. See DOI: 10.1039/b908286g

Table 1 Inhibitory activity of the synthetic compounds **6–10** against binding of [^{125}I]-SDF-1α to CXCR4

Compd	*cyclo*(-Xaa^1-Xaa^2-Arg^3-Nal^4-Gly^5-). Xaa^1-Xaa^2	IC_{50}/μM[a]
2	D-Tyr^1-Arg^2	0.0079
6	D-Phe(4-F)^1-Arg^2	0.22
7	D-Phe(4-F)^1-D-Arg^2	0.31
8	Phe(4-F)^1-Arg^2	0.22
9	Phe(4-F)^1-D-Arg^2	2.2
10	*cyclo*(-D-Tyr^1-Arg^2-Arg^3-Nal^4- Phe(4-F)^5-)	4.4

[a] IC_{50} values are the concentrations for 50% inhibition of the [^{125}I]-SDF-1α binding to CXCR4 transfectants of CHO cells. All data are the mean values for at least three experiments.

Biological results and discussion

SAR of analogues with L/D-Phe(4-F)^1-L/D-Arg^2

Since compound **6**, where D-Tyr^1 of **2** was replaced by 4-fluoro-D-phenylalanine [D-Phe(4-F)] relevant to the new pharmacophore 4-fluorobenzoyl group, showed relatively potent CXCR4-binding activity as reported previously,[26] initially, **6** and its three analogues **7–9**, [L/D-Phe(4-F)^1, L/D-Arg^2]-**2**, were synthesized to evaluate the configuration effects of amino acids at positions 1 and 2 (Table 1). These analogues except for **9** showed high CXCR4 binding activity (IC_{50} = 0.2–0.4 μM, Table 1), although the potencies were much lower than that of **2**. Compound **9** showed moderate potency (IC_{50} = 2.2 μM), suggesting that the combination of Phe(4-F)^1 and D-Arg^2 is not suitable. In addition, compound **10** was synthesized, where Gly^5 of **2** was replaced by Phe(4-F) with maintenance of D-Tyr^1, since both Phe(4-F) and D-Tyr are thought to be important pharmacophore residues. However, compound **10** did not show high potency (IC_{50} = 4.4 μM), probably due to a conformational change.

SAR of analogues with replacement of D-Phe(4-F)^1 of 6 by an aromatic D-amino acid

Based on the configuration of [D-Phe(4-F)^1, L-Arg^2] of **6**, a series of analogues with replacement of D-Phe(4-F)^1 by several aromatic amino acids were synthesized. The order of preference of halogen atoms as a substituent of position 4 on D-Phe^1 is fluorine, chlorine and bromine as shown in activity of **6**, **11** and **12** (IC_{50} = 0.22, 1.2 and 2.3 μM, respectively, Tables 1 & 2). It suggests that a small or electron-withdrawing group is favorable for a substituent of position 4 on D-Phe^1. Next, preference of positions of fluorine on the phenyl ring of D-Phe^1 was investigated. As a result, the order of preference is *ortho*, *meta* and *para*-positions, as shown in activity of **13**, **14** and **6** (IC_{50} = 0.059, 0.088 and 0.22 μM, respectively). In the previous paper, a D-Nal(1)^1-substituted analogue **4** (IC_{50} = 0.043 μM) showed much higher CXCR4 binding activity than a D-Nal^1-substituted analogue, [D-Nal^1]-**2** (IC_{50} > 2.0 μM).[29] Taken together, a *para*-substituent on the phenyl ring of the D-amino acid residue at position 1 is not appropriate for high potency, possibly due to the steric hindrance between the para-substituent on the phenyl ring and CXCR4. In addition, two other analogues were prepared. Compound **15**, [L/D-Phg^1]-**2** (racemic), did not show high CXCR4 binding activity. Compound **16**, [β-(2-thienyl)-D-alanine (D-Thi)^1]-**2**, showed very potent CXCR4 binding activity, suggesting a thienyl group is relatively suitable for the side-chain of the amino acid at position 1. New leads, **13** and **16**, having D-Phe(2-F)^1 and D-Thi^1, respectively, were found although the potencies were approximately one-eighth of that of **2**.

Table 2 Inhibitory activity of the synthetic compounds **11–16** against binding of [^{125}I]-SDF-1α to CXCR4

Compd	*cyclo*(-Xaa^1-Arg^2-Arg^3-Nal^4-Gly^5-). Xaa^1	IC_{50}/μM[a]
2	D-Tyr^1	0.0079
11	D-Phe(4-Cl)^1	1.2
12	D-Phe(4-Br)^1	2.3
13	D-Phe(2-F)^1	0.059
14	D-Phe(3-F)^1	0.088
15	L/D-Phg^1	1.1
16	D-Thi^1	0.056

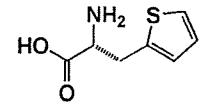

β-(2-thienyl)-D-alanine (D-Thi)

[a] IC_{50} values are the concentrations for 50% inhibition of the [^{125}I]-SDF-1α binding to CXCR4 transfectants of CHO cells. All data are the mean values for at least three experiments.

SAR of analogues with Arg^1-aromatic D-amino acid^2

Since **5**, an analogue with the sequence of Arg^1-D-Nal^2 based on shuffling cationic and aromatic amino acids at positions 1 and 2 of compound **2**, showed high CXCR4 binding activity,[29] a series of analogues with the sequence of Arg^1-aromatic D-amino acid^2 (substitution for D-Nal^2) were synthesized. Among halogen substituents at position 4 on the phenyl ring of D-Phe^2, fluorine is the most suitable, whereas chlorine or bromine is not preferable as shown in activity of **17**,[26] **18** and **19** (IC_{50} = 0.035, 0.79 and 0.57 μM, respectively, Table 3). In addition, a 4-nitro group is not suitable although this group is an electron-withdrawing group, possibly due to steric hindrance (**20**, IC_{50} = 0.94 μM). A 4-hydroxy group with electron-donating action and a 4-amino group with strong electron-donating action is not favorable (**21**, IC_{50} = 0.97 μM, **22**, IC_{50} = 15 μM). As a result, fluorine is the most suitable substituent at position 4 on D-Phe^2 among these atoms and groups. In the investigation of the preference of positions of fluorine on the phenyl ring of D-Phe^2, *para*-position is superior to

Table 3 Inhibitory activity of the synthetic compounds **17–24** against binding of [^{125}I]-SDF-1α to CXCR4

Compd	*cyclo*(-Xaa^1- Xaa^2-Arg^3-Nal^4-Gly^5-). Xaa^1-Xaa^2	IC_{50}/μM[a]
2	D-Tyr^1-Arg^2	0.0079
17	Arg^1-D-Phe(4-F)^2	0.035
18	Arg^1-D-Phe(4-Cl)^2	0.79
19	Arg^1-D-Phe(4-Br)^2	0.57
20	Arg^1-D-Phe(4-NO_2)^2	0.94
21	Arg^1-D-Tyr^2	0.97
22	Arg^1-D-Phe(4-NH_2)^2	15
23	Arg^1-D-Phe(2-F)^2	7.1
24	Arg^1-D-Phe(3-F)^2	6.1

[a] IC_{50} values are the concentrations for 50% inhibition of the [^{125}I]-SDF-1α binding to CXCR4 transfectants of CHO cells. All data are the mean values for at least three experiments.

Table 4 Inhibitory activity of the synthetic compounds **25–31** against binding of [^{125}I]-SDF-1α to CXCR4

Compd	*cyclo*(-D-Tyr^1-**Xaa^2-Xaa^3**-Nal^4-Gly^5-). **Xaa^2-Xaa^3**	IC_{50}/μM[a]
2	Arg^2-Arg^3	0.0079
25	Hph^2-Arg^3	0.075
26	D-Phg^2-Arg^3	6.0
27	Phg^2-Arg^3	0.17
28	His^2-Arg^3	0.037
29	D-His^2-Arg^3	0.035
30	Arg^2-His^3	5.0
31	His^2-His^2	12

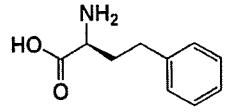

L-homophenylalanine (Hph)

[a] IC_{50} values are the concentrations for 50% inhibition of the [^{125}I]-SDF-1α binding to CXCR4 transfectants of CHO cells. All data are the mean values for at least three experiments.

Table 5 Inhibitory activity of the synthetic compounds **32–37** against binding of [^{125}I]-SDF-1α to CXCR4

Compd	*cyclo*(-**Xaa^1**- **Xaa^2**-Arg^3-Nal^4-Gly^5-). **Xaa^1-Xaa^2**	IC_{50}/μM[a]
2	D-Tyr^1-Arg^2	0.0079
32	Arg^1-His^2	0.40
33	Arg^1-D-His^2	0.96
34	Arg^1-D-Thi^2	1.7
35	Arg^1-D-Tpi^2	8.1
36	Arg^1-D-Hph^2	5.0
37	Arg^1-L/D-Phg^2	5.9

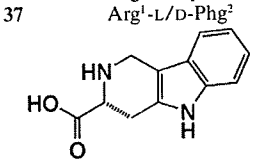

(3*R*)-2,3,4,9-tetrahydro-1*H*-β-carboline -3-carboxylic acid (D-Tpi)

[a] IC_{50} values are the concentrations for 50% inhibition of the [^{125}I]-SDF-1α binding to CXCR4 transfectants of CHO cells. All data are the mean values for at least three experiments.

ortho or *meta* as shown in the activity of **17**, **23** and **24** (IC_{50} = 0.035, 7.1 and 6.1 μM, respectively). In the previous paper, a D-Nal^2-substituted analogue **5** (IC_{50} = 0.045 μM) showed much higher CXCR4 binding activity than a D-Nal(1)^2-substituted analogue, [Arg^1-D-Nal(1)^2]-**2** (IC_{50} > 2.0 μM).[29] Taken together, a *para*-substituent on the phenyl ring of the D-amino acid residue at position 2 is suitable for high potency, possibly due to hydrophobic or π interaction between the *para*-substituent on the phenyl ring and the receptor CXCR4.

SAR of analogues with replacement of Arg^2 of 2 by an aromatic amino acid

Since [D-Tyr^1-Phe(4-F)^2]-**2** showed high CXCR4 binding activity in the previous paper,[26] analogues having incorporation of an aromatic amino acid into position 2 were synthesized. An L-homophenylalanine (Hph)-substituted analogue **25** showed potent CXCR4 binding activity (IC_{50} = 0.075 μM, Table 4), whereas an L-phenylglycine (Phg)-substituted analogue **27** showed lower CXCR4 binding activity (IC_{50} = 0.17 μM), although a D-phenylglycine (D-Phg)-substituted analogue **26** showed even lower CXCR4 binding activity (IC_{50} = 6.0 μM). Since His has both basic and aromatic character, it would be a useful amino acid substitution at position 2. Practically, L- and D-His-substituted analogues **28** and **29** showed high potency (IC_{50} = 0.037 and 0.035 μM, respectively), indicating that the chirality of L/D-His at position 2 does not affect CXCR4 binding. The potencies are approximately one-fourth of that of **2**. Next, we extended the His-substitution to position 3 (Arg^3). Analogues with the sequences of Arg^2-His^3 and His^2-His^3 were synthesized (**30** and **31**, respectively). However, these analogues did not show potent CXCR4 binding activity (IC_{50} = 5.2 and 12 μM, respectively), suggesting that His-substitution for Arg^3 is not appropriate.

SAR of analogues with Arg^1-aromatic-amino acid^2

Among analogues with a combination of the sequences of Arg/His^2-Arg/His^3, **28** having the sequence of His^2-Arg^3 is the most potent compound, with almost the same CXCR4 binding activity as **29** (D-His^2-Arg^3). Thus, **32** and **33**, where D-Tyr^1 of **28** and **29** was replaced by Arg, respectively, were synthesized. However, **32** and **33** are more than 10 fold weaker than **28** and **29** (Table 5), indicating that Arg^1 is not suitable in these analogues. D-Thi, (3*R*)-2,3,4,9-tetrahydro-1*H*-β-carboline-3-carboxylic acid (D-Tpi), D-Hph and L/D-Phg (racemic)-substituted analogues did not show high potency as shown in **34**, **35**, **36** and **37**, respectively. It suggests that these series of analogues with the sequence of Arg^1-aromatic-amino acid^2 are not potent compounds, although **5** and **17** showed high potency.

SAR of analogues with D-Phe(4-F)^1-Arg/His^2-Arg/His^3 or Arg/His^1-D-Phe(4-F)^2-Arg/His^3

Since **6**, [D-Phe(4-F)^1]-**2**, showed moderate CXCR4 binding activity,[26] a series of analogues with the sequence of D-Phe(4-F)^1-Arg/His^2-Arg/His^3 were synthesized (**38**, **39** and **40**). However, significantly potent analogues could not be found (IC_{50} > 10 μM, Table 6). Thus, to interchange the order of positions 1 and 2, a series of analogues with the sequence of Arg/His^1-D-Phe(4-F)^2-Arg/His^3 were synthesized (**41**, **42** and **43**). CXCR4 binding

Table 6 Inhibitory activity of the synthetic compounds **38–43** against binding of [^{125}I]-SDF-1α to CXCR4

Compd	*cyclo*(-**Xaa^1**- **Xaa^2**-**Xaa^3**-Nal^4-Gly^5-). **Xaa^1-Xaa^2-Xaa^3**	IC_{50}/μM[a]
2	D-Tyr^1-Arg^2-Arg^3	0.0079
38	D-Phe(4-F)^1-Arg^2-His^3	22
39	D-Phe(4-F)^1-His^2-Arg^3	10
40	D-Phe(4-F)^1-His^2-His^3	>100
41	Arg^1-D-Phe(4-F)^2-His^3	>100
42	His^1-D-Phe(4-F)^2-Arg^3	5.7
43	His^1-D-Phe(4-F)^2-His^3	>100

[a] IC_{50} values are the concentrations for 50% inhibition of the [^{125}I]-SDF-1 binding to CXCR4 transfectants of CHO cells. All data are the mean values for at least three experiments.

activities of these analogues are relatively weak (IC_{50} > 5 μM), indicating that incorporation of D-Phe(4-F) at position 1 and His-substitution for Arg^3 are not suitable.

Conclusion

In this paper, SAR of several cyclic pentapeptides having CXCR4 binding activity was studied to discover useful lead compounds. (1) Of the analogues with replacement of D-Tyr^1 of **2** by an aromatic D-amino acid, a D-$Phe(2\text{-}F)^1$-substituted analogue, **13**, and a D-Thi^1-substituted analogue, **16**, have potent CXCR4 binding activity. A para-substituent on the phenyl ring of the D-amino acid residue at position 1 is not favorable for high potency. (2) Among a series of analogues based on shuffling cationic and aromatic amino acids at positions 1 and 2, an [Arg^1-D-$Phe(4\text{-}F)^2$]-containing analogue, **17**, showed the most potent CXCR4 binding activity. A *para*-substituent on the phenyl ring of the D-amino acid residue at position 2 is suitable for high potency. (3) Analogues, where Arg^2 of **2** was replaced by L/D-His which have both basic and aromatic characters, have high CXCR4 binding activity. (4) Arg^1-substituted analogues or His^3-substituted analogues are not potent leads. Taken together, in the present study several new leads were found, and aromatic amino acid residues, Phe(2-F), Phe(4-F), Thi and His, were identified to be new pharmacophore residues in addition to Arg, Nal, Nal(1) and Tyr. The present data will be important for the development of CXCR4 antagonists. In future, the introduction of fluorophenyl, thienyl, imidazoyl groups, *etc.* involving the combinational use of the above groups into the cyclic pentapeptide templates and into low molecular weight linear type scaffolds will bring us the development of new-type leads of CXCR4 antagonists. The present data of preferences of the target CXCR4 such as inclination of aromatic and basic groups will be useful to disclose an unknown detail binding mode of CXCR4 and cyclic pentapeptide-type ligands on the cell membrane.

Experimental

Chemistry

Cyclic peptides were synthesized by Fmoc-based solid-phase synthesis followed by cleavage from the resin, cyclization with the diphenylphosphoryl azide and deprotection, as reported previously.[23]

General. The protected peptide resin (0.100 mmol), which was constructed on H-Gly-(2-chloro)trityl resin manually by Fmoc-based solid phase peptide synthesis (SPPS). *t*-Bu for L/D-Tyr and Pbf for L/D-Arg were used for side-chain protection. Fmoc deprotection was achieved by 20% (v/v) piperidine in DMF (10 mL, 2 × 1 min, 1 × 20 min). Fmoc amino acids were coupled by treatment with five equivalents of reagents [Fmoc-amino acid, *N*,*N*′-diisopropylcarbodiimide (DIPCDI) and HOBt·H_2O] to free amino group in DMF (5 mL) for 1.5 h. The constructed protected peptide resin was subjected to AcOH/TFE/CH_2Cl_2 (1 : 1 : 3 (v/v/v), 10 mL) treatment at room temperature for 2 h. After filtration of the residual resin, the filtrate was concentrated under reduced pressure to give a crude protected peptide. To a stirred mixture of the protected peptide and $NaHCO_3$ (57.1 mg, 0.680 mmol) in DMF (41 mL) was added diphenylphosphoryl azide (DPPA, 0.0879 mL, 0.408 mmol) at −40 °C. The mixture was stirred for 36 h with warming to room temperature and filtered. The filtrate was concentrated under reduced pressure to give an oily residue, which was subjected to solid phase extraction over basic alumina in $CHCl_3$-MeOH (9 : 1 (v/v)) to remove inorganic salts derived from DPPA. The resulting cyclic protected peptide was treated with 95% TFA solution for 1.5 h at room temperature. Concentration under reduced pressure and purification by preparative HPLC gave a cyclic peptide.

CXCR4 receptor binding assay[30]

Stable CHO cell transfectants expressing CXCR4 were prepared as described previously.[31] CHO transfectants were detached by treatment with trypsin-EDTA, allowed to recover in complete growth medium (MEM-R, 100 μg/mL penicillin, 100 μg/mL streptomycin, 0.25 μg/mL amphotericin B, 10% FBS (v/v)), and then washed in cold binding buffer (PBS containing 2 mg/mL BSA). For ligand binding, the cells were resuspended in binding buffer at 1×10^7 cell/mL, and 100 μL aliquots were incubated with 0.1 nM of [^{125}I]-SDF-1 (Perkin-Elmer Life Sciences) for 1 h on ice under constant agitation. Free and bound radioligands were separated by centrifugation of the cells through an oil cushion, and bound radioactivity was measured with a gamma-counter (Cobra, Packard, Downers Grove, IL, USA). Inhibitory activity of test compounds was determined based on the inhibition of [^{125}I]-SDF-1 binding to CXCR4 transfectants (IC_{50}).

Acknowledgements

This work was supported by New Energy and Industrial Technology Development Organization (NEDO), Grant-in-Aid for Scientific Research from the Ministry of Education, Culture, Sports, Science, and Technology of Japan, and Health and Labour Sciences Research Grants from Japanese Ministry of Health, Labor, and Welfare.

References

1 K. Tashiro, H. Tada, R. Heilker, M. Shirozu, T. Nakano and T. Honjo, *Science*, 1993, **261**, 600–603.
2 T. Nagasawa, H. Kikutani and T. Kishimoto, *Proc. Natl. Acad. Sci. U. S. A.*, 1994, **91**, 2305–2309.
3 M. Loetscher, T. Geiser, T. O'Reilly, R. Zwahlen, M. Baggiolini and B. Moser, *J. Biol. Chem.*, 1994, **269**, 232–237.
4 B. J. Rollins, *Blood*, 1997, **90**, 909–928.
5 C. C. Bleul, R. C. Fuhlbrigge, J. M. Casanovas, A. Aiuti and T. A. Springer, *J. Exp. Med.*, 1996, **2**, 1101–1109.
6 K. Tachibana, S. Hirota, H. Iizasa, H. Yoshida, K. Kawabata, Y. Kataoka, Y. Kitamura, K. Matsushima, N. Yoshida, S. Nishikawa, T. Kishimoto and T. Nagasawa, *Nature*, 1998, **393**, 591–594.
7 T. Nagasawa, S. Hirota, K. Tachibana, N. Takakura, S. Nishikawa, Y. Kitamura, N. Yoshida, H. Kikutani and T. Kishimoto, *Nature*, 1996, **382**, 635–638.
8 Y. Zhu, Y. Yu, X. C. Zhang, T. Nagasawa, J. Y. Wu and Y. Rao, *Nat. Neurosci.*, 2002, **5**, 719–720.
9 R. K. Stumm, C. Zhou, T. Ara, F. Lazarini, M. Dubois-Dalcq, T. Nagasawa, V. Hollt and S. Schulz, *J. Neurosci.*, 2003, **23**, 5123–5130.

